© Copyright 2019 Nels T. Anderson

A TALE OF TWO STUDIES: SYNTHESES OF SILICON NITRIDE CHEMICAL VAPOR
DEPOSITION PRECURSORS AND DIVALENT LANTHANIDE
N,N-DIMETHYLAMINODIBORANATE COMPLEXES

BY

NELS T. ANDERSON

THESIS

Submitted in partial fulfillment of the requirements
for the degree of Master of Science in Chemistry
in the Graduate College of the
University of Illinois at Urbana-Champaign, 2019

Urbana, Illinois

Adviser:

Professor Gregory S. Girolami

ABSTRACT

Silicon nitride thin films have key industrial applications in the manufacturing of semiconductors, but these applications impose strict requirements on the film growth process. Specifically, the SiN films must be deposited at temperatures below 400 °C to avoid device degradation, and they must be deposited conformally to meet the demand of smaller feature sizes. In chapter 1, the synthesis and deposition of a new precursor for silicon nitride thin films, 1,1-diazido-1-silacyclopent-3-ene (**1**) is described. Precursor **1**, a known compound, was synthesized by treating 1,1-dichloro-1-silacyclopent-3-ene with two equivalents of NaN_3 in acetonitrile, and was purified by distillation under reduced pressures. Deposition experiments were performed in a hot-wall chemical vapor deposition (CVD) reactor show that **1** deposits films at temperatures as low as 400 °C and with excellent conformality in trenches with aspect ratios up to 3.5:1. Elemental characterization of these films, performed by Auger spectroscopy, show that these films contain Si (~10 %) and N (~10 %) in a 1:1 ratio but have high C (~40 %) and O (~40 %) contents, which is likely attributed to the presence of residual moisture and oxygen in the reaction chamber and the slow removal of volatile organic byproducts.

In chapter 2, we describe the syntheses and molecular structures of new Sm^{II} and Tm^{II} *N,N*-dimethylaminodiboranate (DMADB) complexes. Treatment of solutions of $SmI_2(thf)_2$ in thf with $Na(H_3BNMe_2BH_3)$ results in the formation of $Sm(H_3BNMe_2BH_3)_2(thf)_3$ which can be readily converted to the dimethyoxyethane (dme) adduct, $Sm(H_3BNMe_2BH_3)_2(dme)_2$ by treatment with dme. We also show that $Sm(H_3BNMe_2BH_3)_2(thf)_3$ can be prepared by the reduction of the Sm^{III} compound, $Sm(H_3BNMe_2BH_3)_3(thf)$, with KC_8, and that addition of 18-crown-6 to this reaction mixture results in the formation of $Sm(H_3BNMe_2BH_3)_2$(18-crown-6). The new Tm^{II} complexes were synthesized analogously to **1**; treatment of TmI_2 solutions in thf with $Na(H_3BNMe_2BH_3)$

resulted in the formation of 1:1 mixtures of $Tm(H_3BNMe_2BH_3)_2(thf)_3$ and $Tm(H_3BNMe_2BH_3)_2(thf)_2$. IR and ^1H NMR data are reported for all these compounds along with their crystal structures.

Klemperer lab, Dr. Balamargum Kandasamy; I hope you can always see and understand and that all your lunches are good.

I thank our collaborators in the materials department, Dr. John Abelson and his lab members, for all the help on the CVD portion of the silicon nitride project. I especially thank Dr. Tushar Talukdar and Xiaoqing Chu for characterizing all the films I grew and for giving me guidance on the types of deposition experiments to perform. I thank also our collaborators on the f-block metal project at the University of Iowa, Taylor Fetrow and Dr. Scott Daly.

This thesis would not have been possible without the help of the SCS facilities people; much of the data presented in this thesis was collected by them. Specifically, I thank Beth Eves, Crislyn Lu, and Kiran Subedi from the Microanalysis Laboratory and Dean Olsen, the NMR lab manager, who not only stocked the NMR lab with great reading material, but also answered every question I had concerning the NMR instruments and was always available regardless of the time of day to address issues with the instruments. I also thank Danielle Grey and especially Toby Woods of the X-ray laboratory for being quick enough to collect crystal structure data on my often air-sensitive crystals, teaching me how to solve structures in olex2, and giving me ideas on how to crystallize my compounds.

Finally, I thank all my friends and family who helped me carry the emotional burden of this thesis. I thank my roommate Tyler Haddock for soothing my soul with his wonderful music, for opening my eyes to the world of movies, and for all the late-night talks about math and science. I also thank Peter Andersen and Gavin Donley for being two of the best friends a person could have. Last, but certainly not least, I thank my parents, Don and Carol Rodgers, for encouraging me to work hard and be the best I can be and for always and my sister Savannah who never ceases

to remind me that I am a nerd; I hope one day I will have the honor of being in the acknowledgments of your thesis.

TABLE OF CONTENTS

CHAPTER 1: SILYL AZIDE PRECURSORS FOR THE DEPOSITION OF SILICON NITRIDE THIN FILMS

Introduction

Silicon nitride (SiN) thin films have several applications in the manufacturing of microelectronic devices, ranging from gate dielectrics[1-3] to encapsulation layers and diffusion barriers.[4, 5] These applications, however, impose strict requirements on the film growth process. Specifically, the SiN films must be deposited at temperatures below 400 °C to avoid device degradation caused by interfacial reactions,[6-8] and the films must be grown conformally, an attribute that has become increasingly more important as the sizes of device features decrease and the aspect ratios of vias and trenches increase.[9, 10] Conformal films (Figure 1.1a) have a step coverage of 1, where step coverage is defined as the ratio of coating thickness at the bottom of the sidewall of a trench to the coating at the top of the sidewall. In contrast, most film deposition processes result in the growth of subconformal films (Figure 1.1b) which have a step coverages of less than 1; continued deposition results in the formation of a void and a phenomenon called pinch-off (Figure 1.1c).[3]
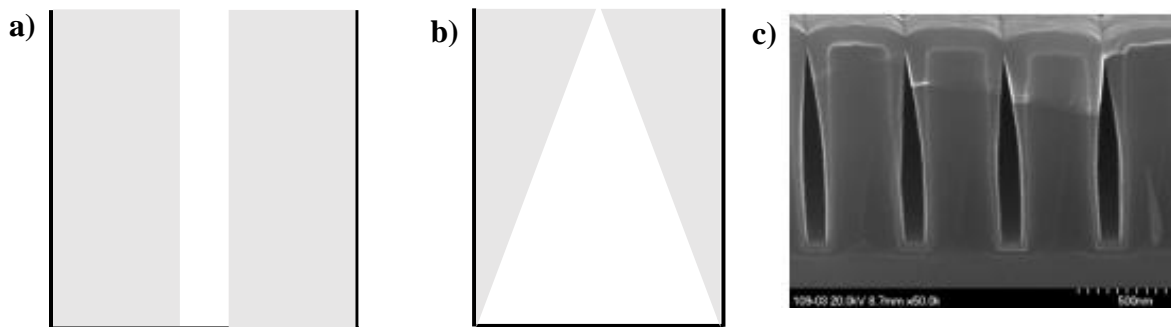

Figure 1.1. (a) conformal (step coverage = 1) and (b) non-conformal (step coverage < 1) film growth in a trench; (c) an illustration of the pinch-off effect, one of the undesirable consequences of non-conformal growth.

One method that has been used successfully to grow conformal films of SiN at temperatures within the thermal budget is atomic layer deposition (ALD) (see Table 1.1).[3, 8, 11, 12] ALD processes typically involve the use of two precursors: for SiN, one precursor is a silicon-containing reagent and the other is a nitrogen-containing reagent. In step one of the ALD process, the first precursor is introduced to the sample chamber, where it reacts with the substrate to form what is essentially a monolayer of reacted precursor. Excess precursor is purged from the chamber and the second precursor is added, which reacts with the monolayer to give the desired material. The chamber is then purged to remove any excess of the second precursor and the cycle is repeated until the desired film thickness is achieved.[13, 14]

Table 1.1. Summary of deposition of SiN films by ALD or CVD. Adapted from reference 8.

Precursors	Temperature (°C)	Step coverage (%)	Aspect ratio	Ref
$Si_3Cl_8 + NH_3$	300-500	>80	60:1	15
$Si_2Cl_6 + NH_3$	350-450	>95	5:1	11
$SiH_4 + N_2$ plasma	250-400	≤ 50	3.5:1	16
$N(SiH_3)_3 + N_2/H_2$ plasma	300, 400	84, 80	2:1	17
$Me_3SiN(SiHMeNMe_2)_2 + N_2$ plasma	250-400	73	5.5:1	18
$Si(SiH_3)_4 + N_2$ plasma	250-300	50	6:1	19
$SiH_3N(^sBu)_2 + N_2$ plasma	100-500	50	4.5:1	8
$N(SiH_3)_3 + N_2/H_2$ plasma[a]	200-400	91	4.2:1	20
$SiH_4 + NH_3$[a]	350	100	1.5:1	21
$SiH_4 + NH_3$[a]	200-400	100	1:1	22

[a] Deposition technique was CVD.

An alternative method for growing SiN films is chemical vapor deposition (CVD). Unlike ALD, which involves the cyclic exposure of a surface to short bursts of two or more precursors, CVD involves the continuous exposure of a surface to a precursor or mixture of precursors (Figure

1.2). The growth of the film can be induced purely thermally, or it can be assisted making use of a non-thermal energy source such as a plasma, which often reduces the temperature at which films can be grown.[23]

1) Transportation of gaseous precursor(s) into reactor and gas-phase reactions

2) Adsorption on substrate

3) Surface reaction with nucleation and island growth

4) Desorption of volatile byproducts
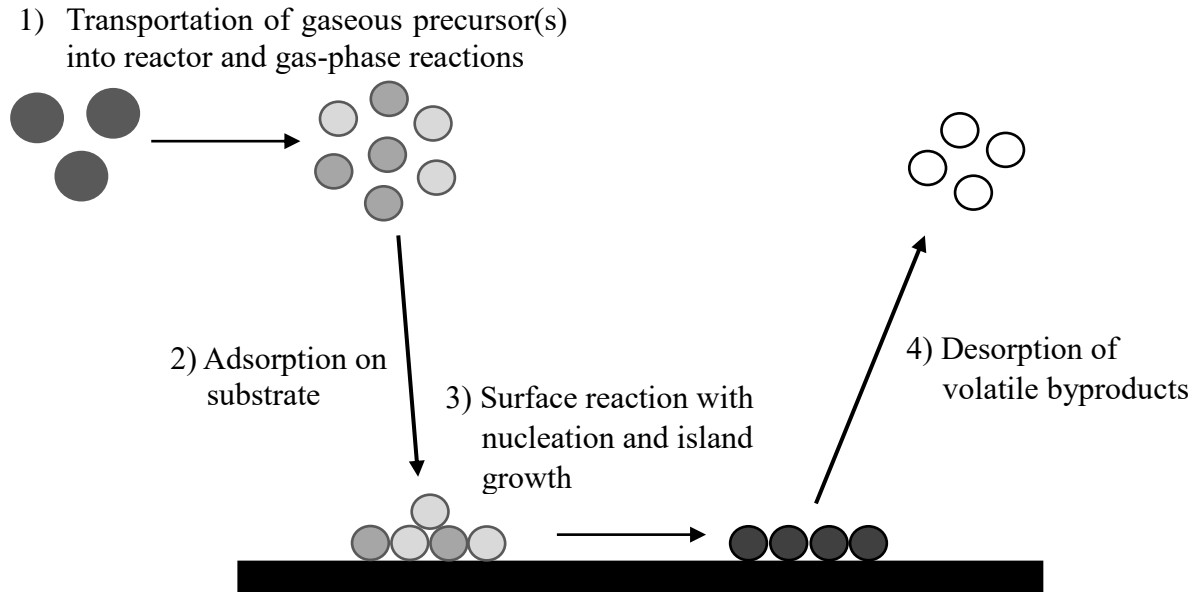
Figure 1.2. General mechanism for the deposition of thin films by chemical vapor deposition (CVD). Figure adapted from reference 23.

Recent attention has focused on depositing SiN films by ALD because this technique is often able to afford films with better conformality than CVD techniques.[16, 17] However, ALD does suffer from disadvantages, one of which is that deposition rates are often quite slow (often on the order of Å/cycle) in comparison to the rates possible with CVD. The slow growth leads to an increased processing time and higher manufacturing costs.[13, 20] This disadvantage makes it worthwhile to reinvestigate CVD methods such as low-pressure CVD (LPCVD)[24] and plasma-enhanced CVD (PECVD)[25] to grow SiN films. What is needed are new precursors that can afford conformal films at lower onset temperatures than those that have been investigated to date.

Although the reactions that occur during the CVD of SiN are not well understood (see references for further discussion on this topic),[1, 26-28] the rate determining step very likely involves breaking a bond. For the systems mentioned in Table 1.1, the strongest bonds are N≡N (BDE = 946 kJ/mol), Si-Cl (BDE = 460 kJ/mol), N-H (BDE = 435 kJ/mol), and Si-H (BDE = 384 kJ/mol).[29] Depositions from precursors with such high BDEs will tend to have high activation energies and high onset temperatures for growth. In addition, the difficulty of breaking these bonds often means that heteroatoms such as hydrogen[29] or chlorine[8, 12] remain in the film.

In contrast, organosilyl azides of the form $R_nSi(N_3)_{4-n}$, where R is a hydrocarbyl substituent, have bonds that are somewhat less strong, such as Si-C (BDE = 368 kJ/mol)[30] and N-C (BDE = 356 kJ/mol).[31] The generally accepted decomposition mechanism for this class of compounds begins with loss of N_2 from an azide group, followed by a Curtius-type rearrangement in which one of the carbon substituents attached to the silicon migrates to the nitrogen that lost N_2.[24, 32-34] Others also suggest that decomposition involves the loss of 3 equivalents of N_2 to form a silylene.[35, 36]

Silicon azides have been explored as CVD precursors to silicon nitrides,[24, 37-39] and we believe that further investigations of this class of molecules could lead to significant advances in the deposition of SiN by CVD, most particularly in lowering the deposition onset temperature.

Results and Discussion

Synthesis of Precursor 1. Motivated by the industrial need for SiN precursors that can deposit conformal films at low temperatures and on reasonable timescales, we decided to test the utility of 1,1-diazido-1-silacyclopent-3-ene (**1**) as a SiN precursor. Precursor **1** is a member of the class of silyl azides which, as mentioned in the introduction, potentially can form silicon nitride

without the need to break N≡N, N-H, or Si-H bonds. We suspected that this attribute would result in lower deposition temperatures.

Precursor **1**, a known compound, was synthesized by the scheme shown below.[40, 41]

Cl
SiCl₃

+ HSiCl₃ →(NEt₃, CuCl / 24 hrs / RT / Et₂O)→ →(Mg / 24 hrs / RT / Et₂O)→ Si(Cl)(Cl) →(2 NaN₃ / 4 hrs / RT / MeCN)→ Si(N₃)(N₃)

Cl

Cl

1
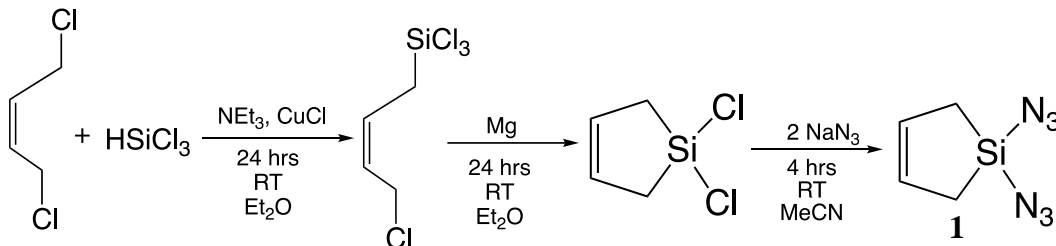
Treatment of a mixture of CuCl, triethylamine, and 1,4-dichloro-2-butene in ether with trichlorosilane results in the formation of 1-trichlorosilyl-4-chloro-2-butene. Subsequent reaction of this compound with Mg produces a Grignard reagent that undergoes ring closure to afford 1,1-dichloro-1-silacyclopent-3-ene. This compound is readily converted to 1,1-diazido-1-silacyclopent-3-ene, **1**, by treatment with two equivalents of NaN₃ in acetonitrile. The identity of **1** was confirmed by ¹H-NMR spectroscopy, IR spectroscopy, and mass spectrometry. After the final distillation of **1** at 84 °C (15 mmHg), trace amounts of Et₂O and MeCN are present, as revealed by ¹H-NMR spectroscopy. Removal of the final traces of solvents can be effected by exposing the final distillate to vacuum at 0 °C for 30 min. The successful removal of the impurities was verified by ¹H-NMR spectroscopy.

Deposition of Films from Precursor 1. Deposition experiments with precursor **1** were performed in the glass apparatus shown in Figure 1.3. The apparatus was connected by means of an L-joint to a Schlenk tube that served as the precursor reservoir. The reservoir was heated in an oil bath and the L-joint was heated with heating tape. The apparatus was connected to a vacuum manifold and heated to the desired deposition temperature in a tube furnace. Gaseous byproducts that exited through the sampling tube were collected in a trap cooled with liquid N₂.

To vacuum/trap

Byproducts

Oven

Precursor inflow

Precursor

Substrate

Base Pressure: ~ 10s of mTorr
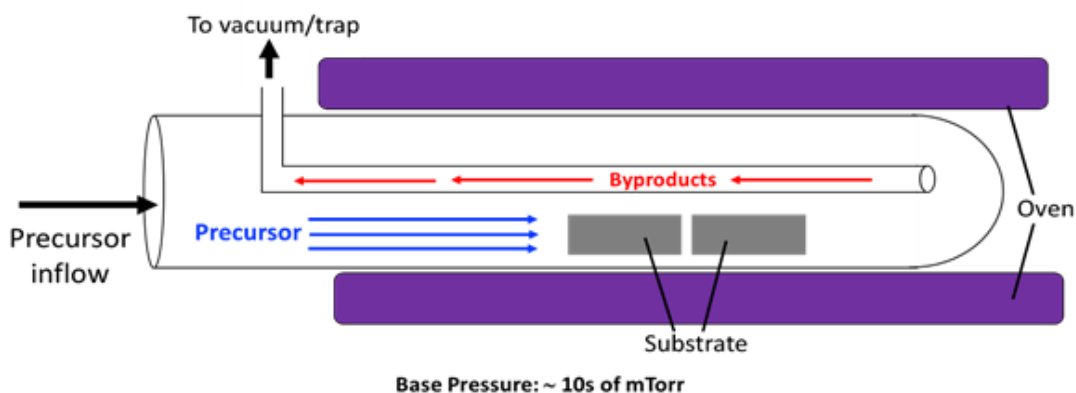
Figure 1.3. Schematic diagram of CVD apparatus used in deposition experiments.

Films were grown from **1** on Si(100) at 400 $^{\circ}$C over a period of 5 h; under these conditions, the films were 56 nm thick (Figure 1.4a) and were quite smooth and non-columnar. The compositions of the films were determined by Auger depth profiles (Figure 1.5). These techniques show that the films contain Si (~10 %) and N (~10 %) in a 1:1 ratio but have high C (~40 %) and O (~40 %) contents. In addition, the refractive index of the films is 1.65 (Figure 1.6), which is between that of SiO_2 ($n = 1.46$) and Si_3N_4 ($n = 2.05$).

For comparison, the precursor $EtSi(N_3)_3$ can deposit films with much lower C and O contents (about 10% each) but only at much higher temperatures of 500 °C (Table 1.2).[24] This experiment was conducted in a better vacuum than that used in our experiment, and it is likely that much of the carbon and oxygen contamination in our film can be attributed to the presence of residual moisture and oxygen in the reaction chamber and the slow removal of volatile organic byproducts.

Additional experiments were conducted on different substrates and at lower deposition temperatures. These experiments show that no film growth occurs on Si(100) at deposition temperatures below 400 °C (Figure 1.4b), but 20 nm films could be grown at 350 °C on gold substrates (Figure 1.7b). Analogous experiments at 400 °C show that **1** deposits films on Au

(Figure 1.7a) that are about 20 nm thicker than those deposited on Si(100) under the same conditions. It is evident from Table 1.2 that, in comparison to deposition temperatures of other CVD precursors, **1** deposits films toward the low end of the temperature spectrum, and that it meets the 400 °C thermal budget requirements for SiN applications in microelectronics.

Figure 1.4. Cross-section SEM image of film grown from **1** on Si(100) surfaces (a) at 400 °C and (b) at 350 °C. Images collected by Tushar Talukdar.
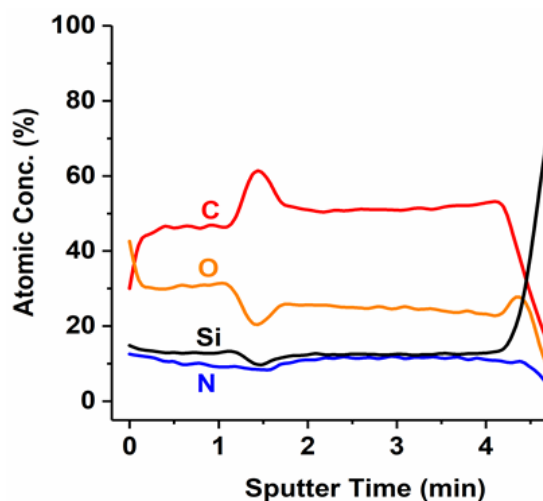
Figure 1.5. Auger depth profiles of films grown from **1** on Si(100) surface at 400 °C. Data collected by Tushar Talukdar.

Table 1.2. Deposition experiments involving other silyl azides.

Precursor	Deposition Method	Deposition Temperature (°C)	Reference
1	Thermal CVD	400	This Work
$EtSi(N_3)_3$	LPCVD	500, 600	[24]
$Et_2Si(N_3)_2$	LPCVD	500, 600	[24]
$(t\text{-}Bu)Si(N_3)_3$	LPCVD	450	[24]
$Me_3Si(N_3)$	PECVD	25-150	[25]
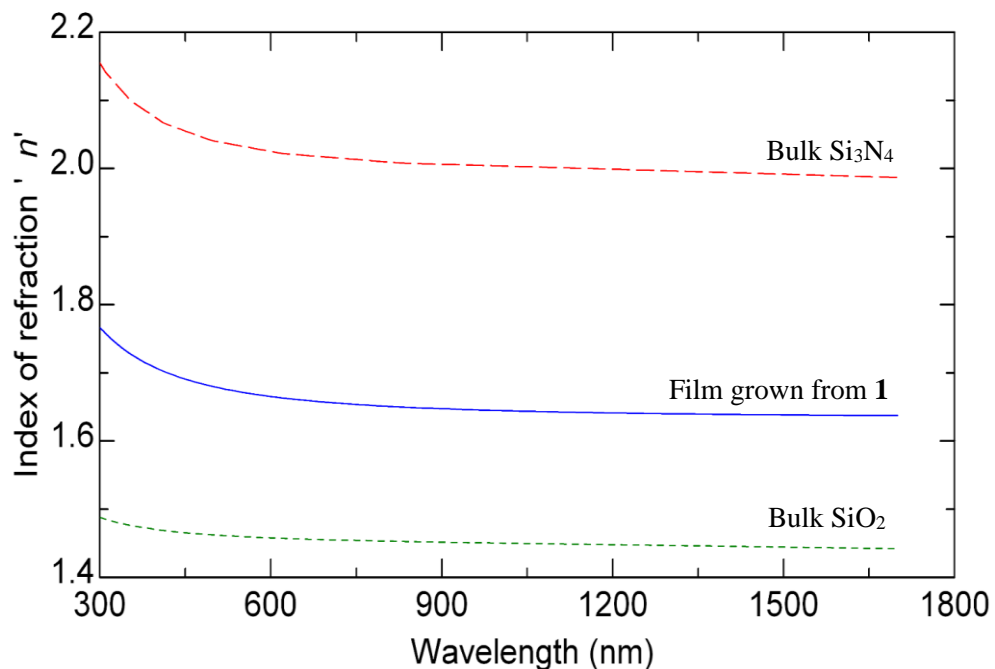
Figure 1.6. Surface ellipsometry traces comparing the refractive indices of the films deposited from **1** at 400 °C (middle, blue) with traces expected for pure SiO_2 (bottom, green) and Si_3N_4 (top, red). The refractive index of films grown from **1** is 82% of the refractive index of Si_3N_4, and 140% of the refractive index of SiO_2. Data collected by Tushar Talukdar.
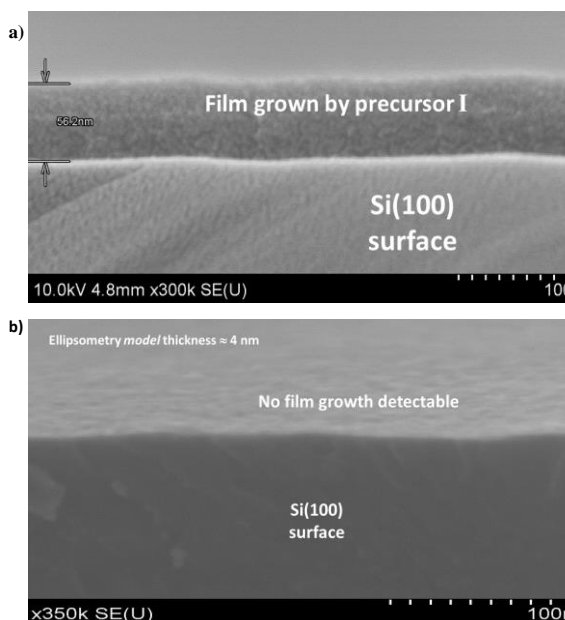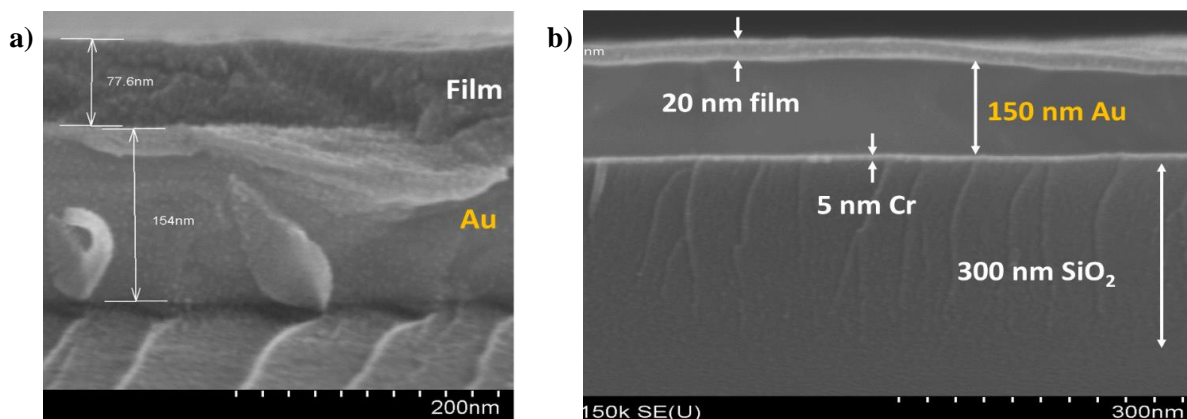

Figure 1.7. Cross-section SEM images of Si_3N_4 grown from **1** on Au (a) at 400 °C and (b) at 350 °C. Images collected by Tushar Talukdar.
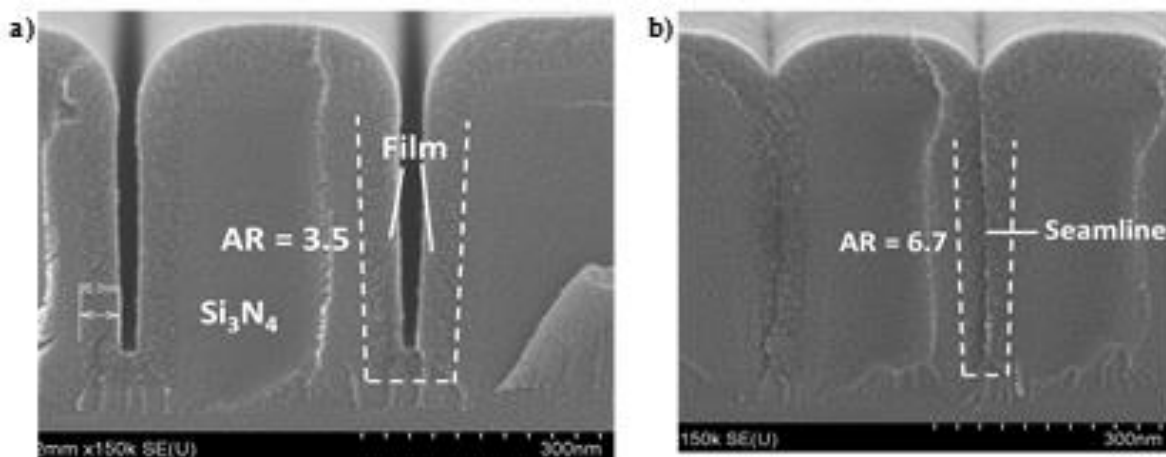
Figure 1.8. Cross-sectional SEM images of Si_3N_4 grown at 400 °C from **1** on Si_3N_4 trenches with an aspect ratio of (a) 3.5 and (b) 6.7. Images collected by Tushar Talukdar.

The conformality of film growth was tested by performing deposition experiments employing Si_3N_4 substrates with pre-made trenches of varying aspect ratios. SEM images of films after deposition revealed that **1** deposits films with excellent conformality at aspect ratios of 3.5 (Figure 1.8a), but grows films with narrow seamlines at an aspect ratio of 6.7 (Figure 1.8b). Unfortunately, no conformality data was reported for the precursors listed in Table 1.2 and, in fact, the few studies of step coverages for the deposition of SiN by CVD report results only for features with very low aspect ratios (see Table 1.1),[21, 22] with one exception: deposition from $N(SiH_3)_3$ by PECVD affords SiN films with a step coverage of 0.91 in features with an aspect ratio of 4.2:1.[20] With respect to SiN films deposited by ALD (Table 1.1), the ability of **1** to fill a feature without a seamline at an aspect ratio of 3.5:1 rivals the best achievements to date.

Synthesis of Precursor 2. Inspired by the positive results above, we sought to make a second SiN precursor, 1,3-di-*tert*-butyl-2,2-diazido-1,3-diaza-2-silacyclopent-4-ene (**2**). The silylene analogue of this compound, 1,3-di-*tert*-butyl-1,3-diaza-2-silacyclopent-4-en-2-ylidene,

9

which can be readily synthesized by treatment of the chlorine analogue with potassium,[42, 43] is quite thermally stable.[42, 44, 45]

The new precursor **2** has been prepared by the reaction sequence shown below.[44] In the first step, the reaction of glyoxal with two equivalents of *tert*-butyl amine affords glyoxal-bis-(*N*-*tert*-butylimine). Reduction of this diimine with excess lithium in thf forms lithium di(*N*-*tert*-butyl)-1,2-ethylenediamide, which is subsequently treated with one equiv. of silicon tetrachloride. Sublimation of the resulting reaction product at 30 °C (10^{-3} Torr) affords white crystals of 1,3-di-*tert*-butyl-2,2-dichloro-1,3-diaza-2-silacyclopent-4-ene which exhibits two peaks in its ^{1}H-NMR spectrum at δ 1.24 (t-Bu) and δ 5.75 (CH).
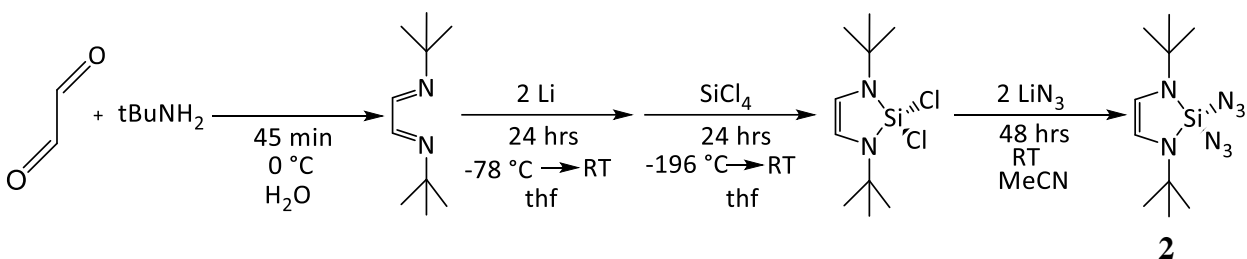
Initial attempts to convert this dichlorosilane into the corresponding diazidosilane were conducted in the same way was that successfully afforded precursor **2**, i.e., by treatment with NaN_3 in acetonitrile. However, ^{1}H and ^{13}C-NMR spectroscopy showed that these reaction conditions gave only small amounts of the desired diazide. We subsequently found that the best conversion was achieved by treating the dichlorosilane with excess LiN_3 in acetonitrile for 48 hours. The successful synthesis of **2** was confirmed by the presence of two new resonances in the ^{1}H-NMR spectrum at δ 1.16 and δ 5.65 consistent with the formation of the diazidosilane product.

Concluding Remarks. We have shown that the precursor 1,1-diazido-1-silacyclopent-3-ene (**1**) deposits films at temperatures of 400 °C with high conformality in trenches with aspect ratios of 3.5:1, but the films have high C and O contents. The deposition temperature of 400 °C is

within the thermal budget for current industrial needs.[6-8] Future experiments with **1** should aim at minimizing oxygen and carbon content in films; specifically, experiments should be conducted in a better vacuum environment than that present in our glass apparatus. The resulting film compositions, refractive indices, and growth rates should be measured as a function of temperature.

Experimental

All operations were carried out in vacuum or under argon using standard Schlenk techniques. All glassware was dried in an oven at 150 °C, assembled hot, and allowed to cool under vacuum before use. Tetrahydrofuran (thf) and pentane were distilled under nitrogen from sodium/benzophenone, and acetonitrile (MeCN) was distilled under nitrogen from boron oxide immediately before use. Krytox grease was used to seal the joints of all reactions involving silicon chlorides or silicon azides. 1,1-Dichloro-1-silacyclopent-3-ene[40] and 1,3-di-*tert*-butyl-2,2-diazido-1,3-diaza-2-sila-4-cyclopentene[44] were prepared by literature routes. NaN_3 (Sigma) was used as received. LiN_3 was dried by heating under vacuum at 50 °C overnight.

The IR spectra were recorded on a Nicolet 200 infrared spectrometer as Nujol mulls between KBr plates. The ^1H NMR data were obtained on a Varian Unity Inova 400 instrument at 400 MHz, Varian Unity U500 instrument at 500 MHz, or a Varian VXR 500 instrument at 500 MHz. ^{13}C NMR data were obtained on a Varian VXR 500 instrument at 125 MHz. ^{29}Si NMR data were obtained on a Carver B500 instrument at 99 MHz. ^1H, ^{13}C, and ^{29}Si NMR chemical shifts are reported in δ units (positive shifts to high frequency) relative to tetramethylsilane. Electron ionization mass spectra were recorded on a Micromass 70-VSE mass spectrometer.

■ **Caution:** *Silyl azides can react with ambient moisture in the air to form the toxic and explosive hydrazoic acid.*[46] *All manipulations should be performed under inert atmosphere.*

1,1-Diazido-1-silacyclopent-3-ene (1).[41] To a 200-mL Schlenk flask charged with NaN_3 (6.0 g, 0.092 mol) and acetonitrile (80 mL) was added 1,1-dichloro-1-silacyclopent-3-ene (4.1 mL, 0.032 mol) in one portion. The mixture was stirred at room temperature for 24 h, and then was treated with Et_2O (30 mL) to cause the immediate formation of a white precipitate. The solution was filtered, and the solvents were removed from the filtrate by distillation at atmospheric pressure. The product, a colorless liquid, was collected by distillation under reduced pressure (84°C/15 Torr). The resulting distillate was cooled to 0 °C, and residual Et_2O and MeCN were removed in vacuum. Yield: 2.1 mL, 2.6 g (47%). IR (cm^{-1}): 3457 br, 3034 m sh, 2964 w, 2925 w, 2900 w, 2150 s, 1605 sh, 1396 s, 1320 br, 1262 m, 1209 m, 1181 m, 1102 s, 945 sh, 821 s, 712 s, 646 s, 574 s. ^{1}H NMR (CDCl$_3$, 20 °C): 1.57 (d, $^3J_{HH}$ = 1.08 Hz, CH_2CH, 4 H), 5.96 (t, $^3J_{HH}$ = 1.11 Hz, CH$_2$CH, 2 H). ^{13}C^{1}H NMR (CDCl$_3$, 20 °C): δ 14.41 (s, CH$_2$CH), 129.20 (s, CH$_2$$C$H). ^{29}Si^{1}H NMR (CDCl$_3$, 20 °C): δ 11.20 (s). MS(EI) [fragment ion, relative abundance]: *m/z* 54 [C$_4$H$_6^+$, 32.0], 70 [100.0], 82 [C$_4$H$_6$Si$^+$, 35.4], 96 [C$_4$H$_6$SiN, 36.7], 124 [C$_4$H$_6$SiN$_3$, 75.8], 137 [C$_4$H$_6$SiN$_4$, 33.6], 166 [C$_4$H$_6$Si(N$_3$)$_2$, 95.6].

1,3-Di-*tert*-butyl-2,2-diazido-1,3-diaza-2-silacyclopent-4-ene (2). A solution of 1,3-di-*tert*-butyl-2,2-dichloro-1,3-diaza-2-silacyclopent-4-ene (0.484 g, 1.73 mmol) in acetonitrile (7 mL) was added to a suspension of LiN$_3$ (0.266 g, 5.42 mmol) in acetonitrile (7 mL). The solution was stirred for 48 h at room temperature. Complete conversion of the chlorine starting material to product was confirmed by NMR spectroscopy. ^{1}H NMR (C$_6$D$_6$, 20 °C): 1.16 (s, NCMe$_3$, 27 H), 5.69 (s, NC$_2$H$_2$N, 2 H). ^{13}C^{1}H NMR (C$_6$D$_6$, 20 °C): δ 30.64 (s, NCMe_3), 51.84 (s, NCMe$_3$), 112.50 (s, NC$_2$H$_2$N).

Deposition Experiments involving Precursor 1. Deposition experiments with 1 were conducted in the CVD apparatus shown in Figure 1.1 and described earlier in this chapter. In a typical experiment, about 0.25 mL of precursor was placed in the reservoir. The pressure inside the apparatus was 10^{-3} mTorr, and a Barnstead Thermolyne tube furnace equipped with a Eurotherm 2116 temperature controller was used to heat the apparatus. Substrates of Si(100), Au, or Si_3N_4 were washed with isopropyl alcohol and acetone and dried in an oven at 150 °C before use. Scanning electron microscope images were obtained on a Hitachi 4800 instrument, surface ellipsometry traces were obtained on a J.A. Woollam M-88 ellipsometer, and Auger surface and depth profiles were obtained on a PEI660 Auger electron spectrometer. All SEM images, surface ellipsometry traces, and AES data were collected by Tushar Talukdar.

References

1.   Nowling, G. R.; Babayan, S. E.; Jakovic, V.; Hicks, R. F., Remote Plasma-Enhanced Chemical Vapour Deposition of Silcion Nitride at Atmospheric Pressure. *Plasma Sources Sci. Technol.* **2002,** *11*, 97-103. DOI: 10.1088/0963-0252/11/1/312

2.   Wil, G. D.; Wallace, R. M.; Anthony, J. M., High-k Gate Dielectrics: Current Status and Materials Properties Considerations. *J. Appl. Phys.* **2001,** *89*, 5243-5275. DOI: 10.1063/1.1361065

3.   Meng, X.; Byun, Y.; Kim, H. S.; Lee, J. S.; Lucero, A. T.; Cheng, L. K., J. , Atomic Layer Deposition of Silicon Nitride Thin Films: A Review of Recent Progress, Challenges, and Outlooks. *Materials* **2016,** *9*, 1-20. DOI: 10.3390/ma9121007

4.   Dussarrat, C.; Girard, J.; Kimura, T.; Tamoki, N.; Sato, Y. Methods for Producing Silicon Nitride Films and Silicon Oxynitride Films by Thermal Chemical Vapor Deposition. U.S. Patent 7,192,626 B2, March 20, 2007.

5.   Rily, F. L., Silicon Nitride and Related Materials. *J. Am. Ceram. Soc.* **2000,** *83*, 245-265. DOI: 10.1111/j.1151-2916.2000.tb01182.x

6.   Ovanesyan, R. A.; Leick, N.; Kelchner, K. M.; Hausmann, D. M.; Agarwal, S., Atomic Layer Deposition of SiC_xN_y Using Si_2Cl_6 and CH_3NH_2 Plasma. *Chem. Mater.* **2017,** *29*, 6269-6278. DOI: 10.1021/acs.chemmater.7b01358

7.   Iyer, R. S.; Seutter, S. M.; Tandon, S.; Sanchez, E. A. C.; Wang, S. Method for Silicon Nitride Chemical Vapor Deposition. US 7,365,029 B2, April 29, 2008.

8.   Faraz, T.; Drunen, M.; Knoops, H. C. M.; Mallikarjunan, A.; Buchanan, I.; Hausmann, D. M.; Henri, J.; Kessels, W. M. M., Atomic Layer Deposition of Wet-Etch Resistant Silicon Nitride Using Di(sec-butylamino)silane and N_2 Plasma on Planar and 3D Substrate Topographies. *ACS Appl. Mater. Interfaces* **2017,** *9*, 1858-1869. DOI: 10.1021/acsami.6b12267

9.   White, L., Design of Precursors for the CVD of Inorganic Thin Films. *Dalton Trans.* **2006**, 5327-5333. DOI: 10.1039/b611848h

10.   Mallek, J. L. Synthesis and Characterization of New Chemical Vapor Deposition Precursors. Ph.D. Thesis, Univeristy of Illinois Urbana Champaign, 2014.

11.   Ovanesyan, R. A.; Hausmann, D. M.; Agarwal, S., Low-Temperature Conformal Atomic Layer Deposition of SiN_x Films Using Si_2Cl_6 and NH_3 Plasma. *ACS Appl. Mater. Interfaces* **2015,** *7*, 10806-10813. DOI: 10.1021/acsami.5b01531

12.   Murray, C. A.; Elliott, S. D.; Hausmann, D.; Henri, J.; LaVoie, A., Effect of Reaction Mechanism on Precursor Exposure Time in Atomic Layer Deposition of Silicon Oxide and Silicon Nitride. *ACS Appl. Mater. Interfaces* **2014,** *6*, 10534-10541. DOI: 10.1021/am5021167

13.   Leskelä, M.; Ritala, M., Atomic Layer Deposition (ALD): From Precursors to Thin Film Structures. *Thin Solid Films* **2002,** *409*, 138-146. DOI: 10.1016/S0040-6090(02)00117-7

14.   George, S. M., Atomic Layer Deposition: An Overview. *Chem. Rev.* **2010,** *110*, 111-131. DOI: 10.1021/cr900056b

15.   Riedel, S.; Sundquvist, J.; Gumprecht, T., Low Temperature Deposition of Silicon Nitride Using Si_3Cl_8. *Thin Solid Films* **2015,** *577*, 114-118. DOI: 10.1016/j.tsf.2015.01.045

16.   King, S. W., Plasma Enhanced Atomic Layer Deposition of SiN_x:H and SiO_2. *J. Vac. Sci. Technol., A* **2011,** *29*, 41501. DOI: 10.1116/1.3584790

17.   Triyoso, D. H.; Hempel, K.; Ohsiek, S.; Jaschke, V.; Shu, J.; Mutas, S.; Schaeffer, J.; Utess, D.; Lenski, M., Evaulation of Low Temperature Silicon Nitride Spacer for High-κ Metal Gate Integration. *ECS J. Solid State Sci. Technol.* **2013,** *2*, N222-N227. DOI: 10.1149/2.022311jss

18.   Park, J.-M.; Jang, S. J.; Yusup, L. L.; Lee, W.-J.; Lee, S.-I., Plasma-Enhanced Atomic Layer Deposition of Silicon Nitride Using a Novel Silylamine Precursor. *ACS Appl. Mater. Interfaces* **2016,** *8*, 20865-20871. DOI: 10.1021/acsami.6b06175

19.   Weeks, S.; Nowling, G.; Fuchigami, N.; Bowes, L., K., Plasma Enhanced Atomic Layer Deposition of Silicon Nitride Using Neopentasilane. *J. Vac. Sci. Technol., A* **2016,** *34*, 01A140. DOI: 10.1116/1.4937993

20.   Lee, W.-J.; Choa, Y.-H., Novel Plasma Enhanced Chemical Vapor Deposition of Highly Conformal SiN Films and their Barrier Properties. *J. Vac. Sci. Technol., B* **2018,** *36*, 022201. DOI: 10.1116/1.5002660

21.   Wang, Q.; Ward, S.; Gedvilas, L.; Keyes, B.; Sanchez, E.; Wang, S., Conformal Thin-Film Silicon Nitride Deposited by Hot-Wire Chemical Vapor Deposition. *Appl. Phys. Lett.* **2004,** *84*, 338. DOI: 10.1063/1.1640803

22.   Okada, S.; Matsumura, H., Improved Properties of Silicon Nitride Films Prepared by the Catalytic Chemical Vapor Deposition Method. *Jpn. J. Appl. Phys.* **1997,** *36*, 7035. DOI: 10.1143/JJAP.36.7035

23.   Jones, C. A.; Hitchman, M. L., Overview of Chemical Vapor Deposition. In *Chemical Vapor Deposition: Precursor, Processes and Applications*, Jones, C. A.; Hitchman, M. L., Eds. Royal Society of Chemistry: 2009; pp 1-36.

24.   Roberts, D. A.; Hochlberg, A. K.; O'Meara, D. L.; Rusnak, F.; Hockenhull, H., The LPCVD of Silicon Nitride Films from Alkylazidosilanes. *Mat. Res. Soc. Symp. Proc.* **1991,** *24*, 515-520.

25.   Janča, J.; Nečasová, M.; Šikola, T., Plasma-Deposited Silicon Nitride Films in HMDS (Hexamethyldisilazane) Vapours. *Acta Phys. Slov.* **1983,** *33*, 187-193.

26.   Crabtree, K. N.; Martinez, O.; McCarthy, M. C., Detection of Two Highly Stable Silicon Nitrides: HSiNSi and H_3SiNSi. *J. Phys. Chem. A* **2013,** *117*, 11282-11288. DOI: 10.1021/jp4068119

27.   Tachibana, A.; Yamaguchi, K.; Kawauchi, S.; Kurosaki, Y.; Yamabe, T., SiH_3 Radical Mechanisms for Si-N Bond Formation. *J. Am. Chem. Soc.* **1992,** *114*, 7504-7507. DOI: 10.1021/ja00045a025

28.   Hirao, T.; Setsune, K.; Kitagawa, M.; Manabe, Y.; Wasa, K.; Kohiki, S., Role of Ions and Radical Species in Silicon Nitride Deposition by ECR Plasma CVD Method. *Jpn. J. Appl. Phys.* **1987,** *26*, 1544-1546. DOI: 10.1143/JJAP.26.L544

29.   Kaloyeros, A. E.; Jove, F. A.; Goff, J.; Arkles, B., Review-Silicon Nitride and Silicon Nitride-Rich Thin Film Technologies and Related Applications. *ECS J. Solid State Sci. Technol.* **2017,** *6*, 691-714. DOI: 10.1149/2.0011710jss

30.   Walsh, R. W., Bond Dissociation Energy Values in Silicon Containing Compounds and Some of their Implications. *Acc. Chem. Res.* **1981,** *14*, 246-252. DOI: 10.1021/ar00068a004

31.   Luo, Y.-R.; Cheng, J.-P., Table 3. Bond Dissociation Energies in Polyatomic Molecules. In *CRC Handbook*, 100 ed.; Rumble, J. R., Ed. Boca Raton, FL, 2019.

32.   Reichle, W. T., Preparation, Properties, and Thermal Decomposition Products of Organoazides of Silicon, Germanium, Tin, Lead, Phosphorus, and Sulfur. *Inorg. Chem.* **1964,** *3*, 402-406. DOI: 10.1021/ic50013a021

33.   Parker, D. R.; Sommer, L. H., Photolysis of Silyl Azides. Generation and Reactions of Silicon-Nitrogen (pπ-pπ) Doubly Bonded Intermediates [$R_2Si=NR$]. *J. Am. Chem. Soc.* **1976,** *98*. DOI: 10.1021/ja00418a055

34.   Bertrand, G.; Majoral, J.; Baceiredo, A., Photochemical and Thermal Rearrangement of Heavier Main-Group Element Azides. *Acc. Chem. Res.* **1986,** *19*, 17-23. DOI: 10.1021/ar00121a003

35.   Patyk, A. S., W.; Gauss, J.; Cremer, D., Dimethyldioxasilirane. *Angew. Chem. Int. Ed.* **1989,** *28*, 898-900. DOI: 10.1002/anie.198908981

36.   Herges, R.; Starck, F., Synthesis and Fragmentation of 2,2-Diazido-1,3,2-dioxasila-5-cycloheptenes. The Chemical Vapor Depsotion of SiO_2. *J. Am. Chem. Soc.* **1996,** *118*, 12752-12757. DOI: 10.1021/ja9615886

37.   Hochberg, A. K.; Beach, S.; O'Meara, D. L.; Roberts, D. A. Deposition of Silicon Nitride Films from Azidosilane Sources. U.S. Patent 4992299, February 12, 1991.

38.   Ishikawa, M.; Machida, H.; Sudo, H. Film Forming Material, Film Forming Method and Device. Japanese Patent JP2011009479A, January 1, 2011.

39.   LaVoie, A.; Saly, M. J.; Odedra, R. D.; Kanjolia, R. Precursors for Plasma Activated Conformal Film Deposition. U.S. Patent US20130210241A1, August 15, 2013.

40.   Damrauer, R.; Simon, R., Synthesis of 3-Methylene-1,1-dichlorosilylcyclobutane and 1,1-Dichlorosilacyclopent-3-ene. *J. Organomet. Chem.* **1990,** *391*. DOI: 10.1016/0022-328X(90)80150-X

41.   Khabashesku, V. N.; Balaji, V.; Boganov, S. E.; Nefedov, O. M.; Michl, J., Matrix Isolation of Silacyclopentadienes: UV-Vis and IR Spectra and Photochemical Interconversion. *J. Am. Chem. Soc.* **1994,** *116*, 320-329. DOI: 10.1021/ja00080a037

42.   Denk, M.; Lennon, R.; Hayashi, R.; West, R.; Belyakov, A. V.; Verne, H. P.; Haaland, A.; Wagner, M.; Metzler, N., Synthesis and Structure of a Stable Silylene. *J. Am. Chem. Soc.* **1994,** *116*, 2691-2692. DOI: 10.1021/ja00085a088

43.   Neumann, E. Transition Metal Complexes with P,N-Ligands and Silylenes: Synthesis and Catalytic Studies. University of Basel, 2006.

44.   Haaf, M.; Schmiedl, A.; Schmedake, T. A.; Powell, D. R.; Millevolte, A. J.; M., D.; West, R., Synthesis and Reactivity of a Stable Silylene. *J. Am. Chem. Soc.* **1998,** *120*, 12714-12719. DOI: 10.1021/ja9733999

45.   Denk, M.; Hayashi, R. K.; West, R., Reaction of a Stable Silylene with Covalent Azides: A New Synthesis for Silamines. *J. Am. Chem. Soc.* **1994,** *116*, 10813-10814. DOI: 10.1021/ja00102a068

46.   Wiss, J.; Fleury, C.; Heuberger, C.; Onken, U., Explosion and Decomposition Characteristics of Hydrazoic Acid in the Gas Phase. *Org. Process Res. Dev.* **2007,** *11*, 1096-1103. DOI: 10.1021/op7000645

CHAPTER 2: SYNTHESIS AND CHARACTERIZATION OF DIVALENT SAMARIUM AND THULIUM *N,N*-DIMETHYLAMINODIBORANATES

Introduction

Divalent lanthanoid chemistry has been traditionally dominated by the three easiest lanthanoids to reduce, namely Eu, Yb, and Sm, even though divalent complexes of lanthanoids with reduction potentials more negative than Sm were described as early as the 1950s.[1] It was not until the late 90s, however, when Bochkarev et al. isolated the first molecular Tm^{II} complex, TmI$_2$(dme)$_3$, that there was a significant expansion in the known divalent chemistry of lanthanoids other than Eu, Yb, and Sm.[2] Since this finding, Tm^{II} chemistry has been expanded to include phospholyl ligands,[3, 4] borohydrides,[5] and organic ligands,[6] and has proven to be useful for the reduction of unsaturated hydrocarbons[7] and ketones.[8]

One motivation for exploring divalent lanthanoid chemistry relates to the production of high purity f-block metals, which have several key industrial applications.[9-13] The separation and purification of f-block metals in their +3 oxidation states can be achieved by extraction and chromatographic methods,[14] but an alternative method to effect these separations takes advantage of differences in the +3/+2 reduction potentials. Generally, these separations involve treating mixtures of lanthanoids with a reducing agent such as hydrogen or an alkali metal, followed by precipitation of the reduced species; such methods have proven successful for the purification of Eu,[11, 15-17] Yb,[18-20] and Sm.[21, 22]

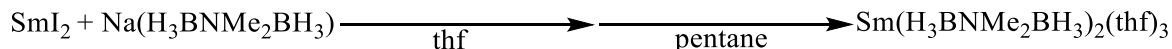The reduction of Ln^{III} to Ln^{II} by the addition of a reducing agent has also been used to access other Ln^{II} complexes, some even containing divalent states less accessible than Tm. For example, Evans et al. synthesized divalent complexes of all the lanthanoids by treating cooled solutions of 18-crown-6 or [2.2.2]cryptand and Ln(C$_5$H$_4$SiMe$_3$)$_3$ with K or KC$_8$ to form [K(18-

crown-6)][Ln(C$_5$H$_4$SiMe$_3$)$_3$] or [K([2.2.2]cryptand)][Ln(C$_5$H$_4$SiMe$_3$)$_3$].[23-25] In a similar manner, Jaroschik et al. showed that [K(18-crown-6)][(C$_5$H$_2$(t-Bu)$_3$)$_2$Dy(BH$_4$)] could be made by the reduction of (C$_5$H$_2$(t-Bu)$_3$)$_2$Dy(BH$_4$) by KC$_8$.[26]

Our group has recently begun to study divalent lanthanide complexes of a new class of multidentate borohydride ligands, the aminodiboranates. In previous work, we described the syntheses and molecular structures of Eu^{II} and Yb^{II} *N,N*-dimethylaminodiboranate (DMADB) complexes and showed that these complexes could be prepared by either salt metathesis with the appropriate diiodide salt or by reduction of LnCl$_3$ by the DMADB ligand.[27] Efforts to obtain a Sm^{II} compound by the latter method were unsuccessful. Here, we show that divalent lanthanide chemistry with DMADB can in fact be extended to include Sm and Tm by reporting the synthesis, characterization, and molecular structures of several Sm^{II} and Tm^{II} DMADB complexes.

Results and Discussion

Synthesis of Ln(H$_3$BNMe$_2$BH$_3$)$_2$ Compounds from Ln^{II} Starting Materials. A general method to prepare LnI$_2$ starting materials is by action of I$_2$ or 1,2-diiodoethane on the powdered metal.[28, 29] For samarium, the resulting compound SmI$_2$(thf)$_2$ can be isolated and stored under an inert atmosphere as the powder and used as needed. This diiodide serves as a useful starting material: the divalent Sm compound Sm(H$_3$BNMe$_2$BH$_3$)$_2$(thf)$_3$ (**1**), can be prepared by salt-metathesis between SmI$_2$(thf)$_2$ and Na(H$_3$BNMe$_2$BH$_3$) in tetrahydrofuran:

$$\text{SmI}_2 + \text{Na(H}_3\text{BNMe}_2\text{BH}_3) \xrightarrow{\text{thf}} \xrightarrow{\text{pentane}} \text{Sm(H}_3\text{BNMe}_2\text{BH}_3)_2(\text{thf})_3$$

The product was isolated from the crude reaction mixture by extraction with pentane, and crystals were obtained by cooling a concentrated solution in pentane to -20 °C. The samarium compound **1** is reddish purple and crystallizes as the tris thf adduct.

19

Adducts of $Sm(H_3BNMe_2BH_3)_2$ with ethers other than thf can also be made. Thus, treatment of **1** with excess 1,2-dimethoxyethane (dme) results in the formation of a bright red solution from which bright red crystals of $Sm(H_3BNMe_2BH_3)_2(dme)_2$ (**2**) can be isolated. Unlike the thf adduct, **2** is essentially insoluble in pentane. In addition, as we will show in the next section, the crown ether adduct, $Sm(H_3BNMe_2BH_3)_2(18\text{-crown-}6)$ (**3**), can be made by reduction of $Sm(H_3BNMe_2BH_3)_3$ with KC_8 in the presence of 18-crown-6.

$$Sm(H_3BNMe_2BH_3)_2(thf)_3 \xrightarrow{\quad dme \quad} Sm(H_3BNMe_2BH_3)_2(dme)_2$$

Thulium(II) DMADB compounds can be obtained in a fashion similar manner to the Sm compound, however, except that $TmI_2(thf)_x$ should be prepared and used immediately due to its tendency to oxidize in solution and in the presence of UV light.[2] Specifically, treatment of $TmI_2(thf)_x$ with and $Na(H_3BNMe_2BH_3)$ in thf, followed by crystallization from pentane, affords brown crystals of $Tm(H_3BNMe_2BH_3)_2(thf)_{2.5}$ (**4/5**).

$$TmI_2 + Na(H_3BNMe_2BH_3) \xrightarrow{\quad thf \quad} \xrightarrow{\quad pentane \quad} Tm(H_3BNMe_2BH_3)_2(thf)_{2.5}$$

As we will show below, this compound crystallizes as a mixture of the bis thf adduct **4** and the tris thf adduct **5**. The analogous reaction of **4** and **5** with dme generates a purple solution which presumably contains a dme adduct of $Tm(H_3BNMe_2BH_3)_2$. Solvent diffusion or vapor diffusion of pentane into these solutions have so far resulted in the formation of a purple powder instead of crystals.

Tm^{II} compounds have been proposed to be useful as powerful reducing agents in organic synthesis,[8] but can be difficult to handle: they often reduce solvent molecules and sometimes even N_2.[7, 30, 31] In comparison to other Tm^{II} compounds, $Tm(H_3BNMe_2BH_3)_2(thf)_{2.5}$ is remarkably stable: although dry samples are spontaneously flammable in air, it does not react with N_2 and does not reduce ethereal solvents.
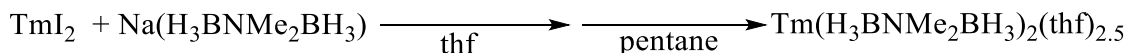
Synthesis of Ln(H₃BNMe₂BH₃)₂ Compounds from Ln^III Starting Materials. We have found that the samarium(II) compound **1** can also be made by reduction of trivalent starting materials. Thus, treatment of $Sm(H_3BNMe_2BH_3)_3(thf)$ with one equiv of KC_8 causes the reaction mixture to change color from pale yellow to dark red. Adding pentane to the reaction mixture and cooling to -20 °C results in the formation of a mixture of red and white crystals. The red crystals were identified as **1** by X-ray diffraction; the white crystals are presumably $K(H_3BNMe_2BH_3)$.

$$Sm(H_3BNMe_2BH_3)_3(thf) + KC_8 \xrightarrow{\quad thf \quad} Sm(H_3BNMe_2BH_3)_2(thf)_3$$
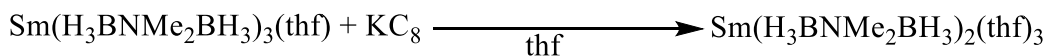
We next investigated whether performing this reaction in the presence of 18-crown-6 would lead to the salt $[K(18\text{-crown-}6)_x][Sm(H_3BNMe_2BH_3)_3]$, a reaction that would be analogous to several noted by Evans et al. for certain cyclopentadienyl complexes,[23-25] as described in the introduction. We find that treatment of solutions of $Sm(H_3BNMe_2BH_3)_3(thf)$ in Et_2O with suspensions of 18-crown-6 and KC_8 in Et_2O gives a different outcome: a dark precipitate is formed that dissolves to form a red solution in thf. Cooling this solution to -20 °C gives crystals of the new Sm^II compound $Sm(H_3BNMe_2BH_3)_2(18\text{-crown-}6)$ (**3**), in which the crown ether is bound to samarium instead of potassium. This compound is insoluble in Et_2O and pentane.

Analogous efforts to make a neodymium(II) complex by treating solutions of $Nd(H_3BNMe_2BH_3)_3(thf)$ with KC_8 or with KC_8 and 18-crown-6, at temperatures between -78 °C and room temperature, result in no color change of the reaction mixtures. This finding suggests either that no divalent species is formed, or that it is formed transiently and immediately decomposes in solution to trivalent products.

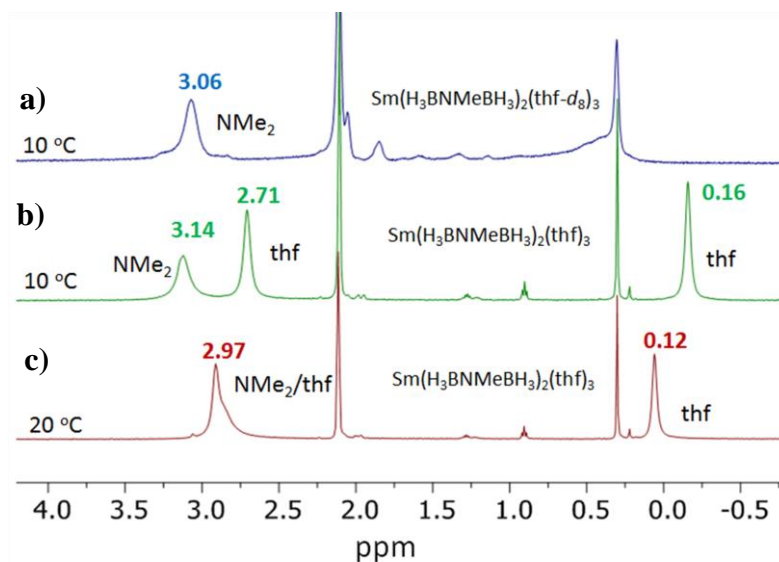**NMR and IR Studies of Ln^II Compounds.** The ^1H NMR spectrum of

Figure 2.1. Comparison of ^{1}H NMR spectra of $Sm(H_3BNMe_2BH_3)_2(thf\text{-}d_8)_3$ at 10 °C (a) and $Sm(H_3BNMe_2BH_3)_2(thf)_3$, **1**, in toluene-$d_8$ at 10 °C (b) and 20 °C (c).

$Sm(H_3BNMe_2BH_3)_2(thf)_3$, **1**, at 10 °C in toluene-d_8 consists of three equal-intensity broad peaks at δ 3.14, 2.71, and 0.12 (Figure 2.1b). (These chemical shifts are temperature dependent, as expected for a paramagnetic compound, and at room temperature the first two of these peaks are accidentally superimposed at δ 2.97 (Figure 2.1c)). Initial attempts to assign the peaks were made by adding a small amount of thf-d_8 to a solution of **1** in toluene-d_8, with the expectation that ligand exchange would afford the thf-d_8 adduct $Sm(H_3BNMe_2BH_3)_2(thf\text{-}d_8)_3$, and that two of the three peaks would disappear and be replaced by two peaks due to free thf. However, this experiment resulted instead in the disappearance of all three resonances and the appearance of a new singlet near δ 5.00. The addition of thf-d_8 also causes the ^{11}B NMR chemical shift at room temperature to change from δ 256 to 217. These results strongly suggest that addition of thf-d_8 does more than replace the coordinated thf ligands: the presence of excess thf must convert **1** into a different compound, presumably one having more than three thf ligands per metal center.

22
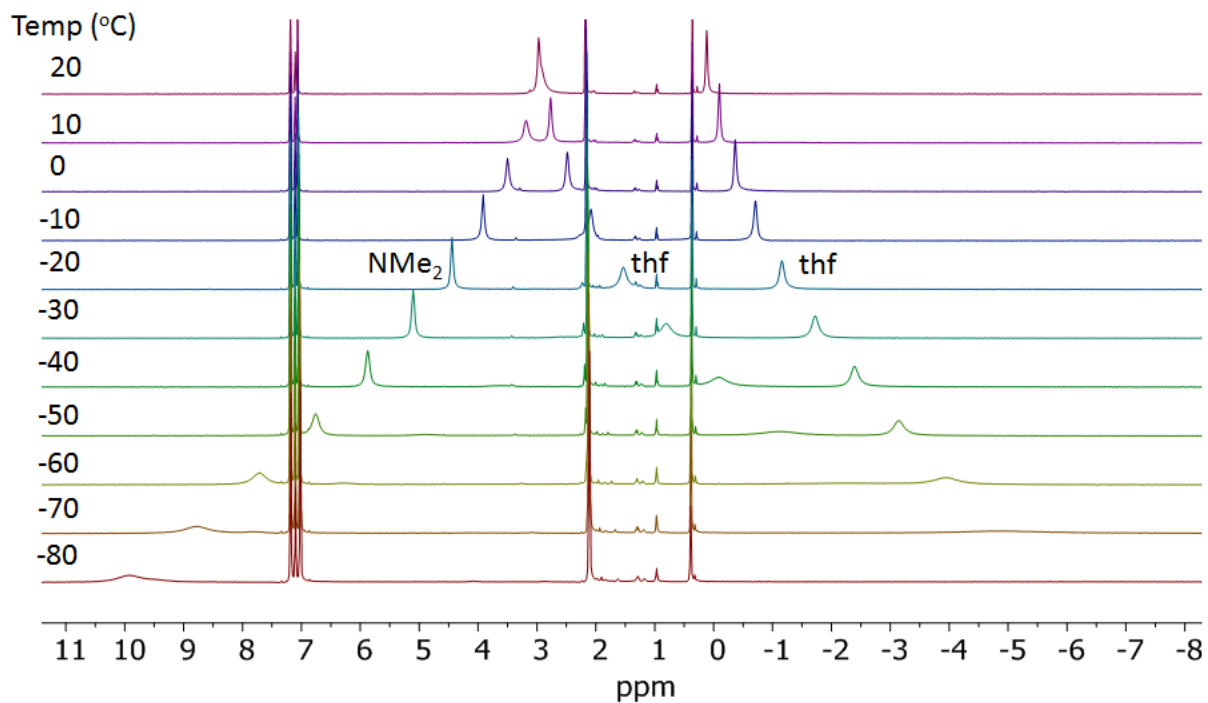
Figure 2.2. VT ^{1}H NMR spectra of Sm(H$_3$BNMe$_2$BH$_3$)$_2$(thf)$_3$, **1**, in toluene-d_8.

Therefore, peak assignments were made by comparison with the NMR spectra of Sm(H$_3$BNMe$_2$BH$_3$)$_2$(thf-d_8)$_3$, which was prepared by treating **1** with thf-d_8 followed by removal of the solvent in vacuum. The ^{1}H NMR spectrum of this deuterated isotopolog in toluene-d_8 at 10 °C (Figure 2.1a) contains only one singlet at δ 3.14, which matches one of the three peaks seen for the protio analog. This peak must therefore be assigned to the NMe$_2$ protons. It follows then that the other two resonances seen at δ 2.71 and 0.12 in the NMR spectrum of the protio isotopolog can be assigned to the thf ligands. The BH$_3$ protons are not observed, evidently because the proximity of these protons to the paramagnetic center causes the BH$_3$ resonance to be significantly broadened and shifted, as has been noted in other f^6 and f^7 lanthanide DMADB complexes.[32] Additionally, the 1:1:1 ratio of peak integrals seen for the three resonances for the protio isotopolog implies that, in solution, all the DMADB ligands are chemically equivalent, as are all of the THF
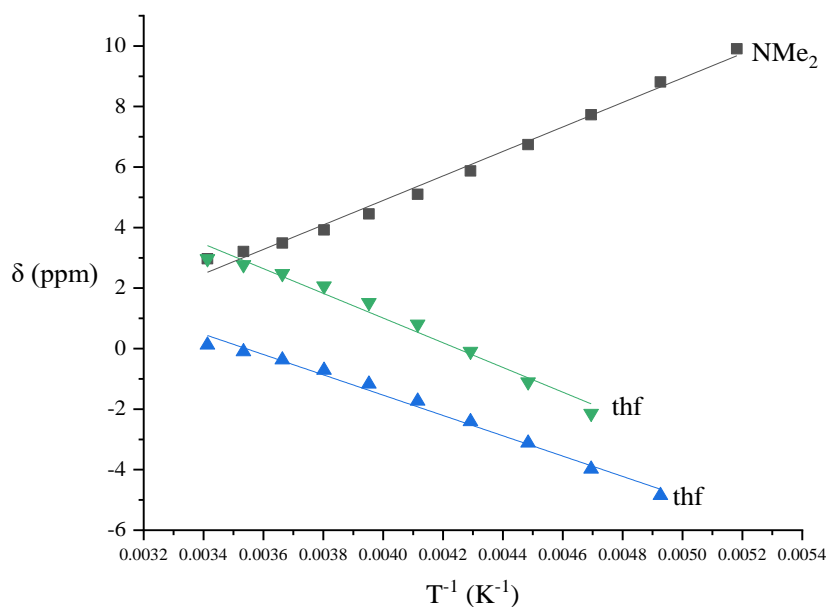
Figure 2.3. Curie plots for the VT-NMR experiment of **1**. Solid lines denote lines of best of fit.

ligands. This result is inconsistent with the solid-state structure of **1** (see below) and shows that this complex is dynamic in solution. In particular, the axial and equatorial thf ligands must be exchanging at a rate faster than the NMR time scale at 10 °C.

The peak assignments were further confirmed from Curie plots of the ^{1}H NMR chemical shifts of **1** as a function of inverse absolute temperature, T^{-1} (Figure 2.2). Magnetic materials that follow Curie behavior have magnetic moments, χ, and consequently NMR shifts, that are linearly dependent on T^{-1}. When T = infinity, the contribution of paramagnetic effects (δ_{para}) to the chemical shift is zero because there is an equal Boltzmann distribution across spin states (and therefore no net spin polarization). In the absence of other effects such as TIP (see below), the chemical shift in the limit $T^{-1} = 0$ (i.e., the y-intercept of the Curie plot) depends only on the contribution from diamagnetic effects (δ_{dia}). This method has been successfully used to assign the peaks in the ^{1}H-NMR spectrum of bis-porphyrin actinide complexes.[33]
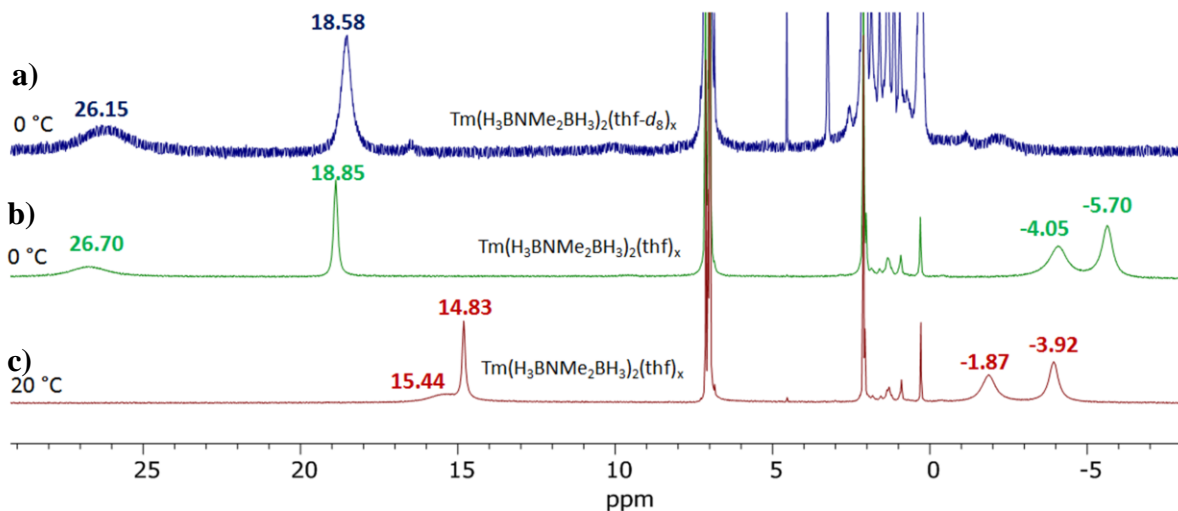
Figure 2.4. Comparison of ^{1}H NMR spectra of Tm(H$_3$BNMe$_2$BH$_3$)$_2$(thf-d_8)$_{2.5}$ at 0 °C (a) and

Tm(H$_3$BNMe$_2$BH$_3$)$_2$(thf)$_{2.5}$, **4/5**, at 0 °C (b) and 20 °C (c) in toluene-d_8.

Here, the *y*-intercepts for the peaks in the Curie plots of **1** (Figure 2.3) imply that δ_{dia}= -11,

11, and 16 for NMe$_2$, thf, and thf respectively which are all far from the expected diamagnetic

shifts of these species. One possible explanation to this deviation is Van Vleck temperature

independent paramagnetism (TIP); this phenomenon, for example, causes species containing the

isoelectronic Eu^{III} ion to exhibit similar deviations from Curie behavior.[34]

It is also worth noting that all three ^{1}H NMR peaks broaden at low temperatures. The

linewidths of paramagnetic species generally become broader at lower temperatures, but we cannot

rule out the possibilities that some of the broadening is due to slowing of an exchange process at

temperatures near -80 °C, or to decreases in molecular tumbling times caused by an increase in the

viscosity of the NMR solvent.[35]

The ^{1}H NMR spectrum of the Tm(H$_3$BNMe$_2$BH$_3$)$_2$(thf)$_x$ co-crystals (**4/5**) at 0 °C in toluene-

d_8 contains four peaks at δ 26.15, 18.58, -4.03, and -5.60 (Figure 2.4b). The number of peaks

suggests that **4** and **5** are exchanging with one another rapidly: dissociation of thf from the tris thf
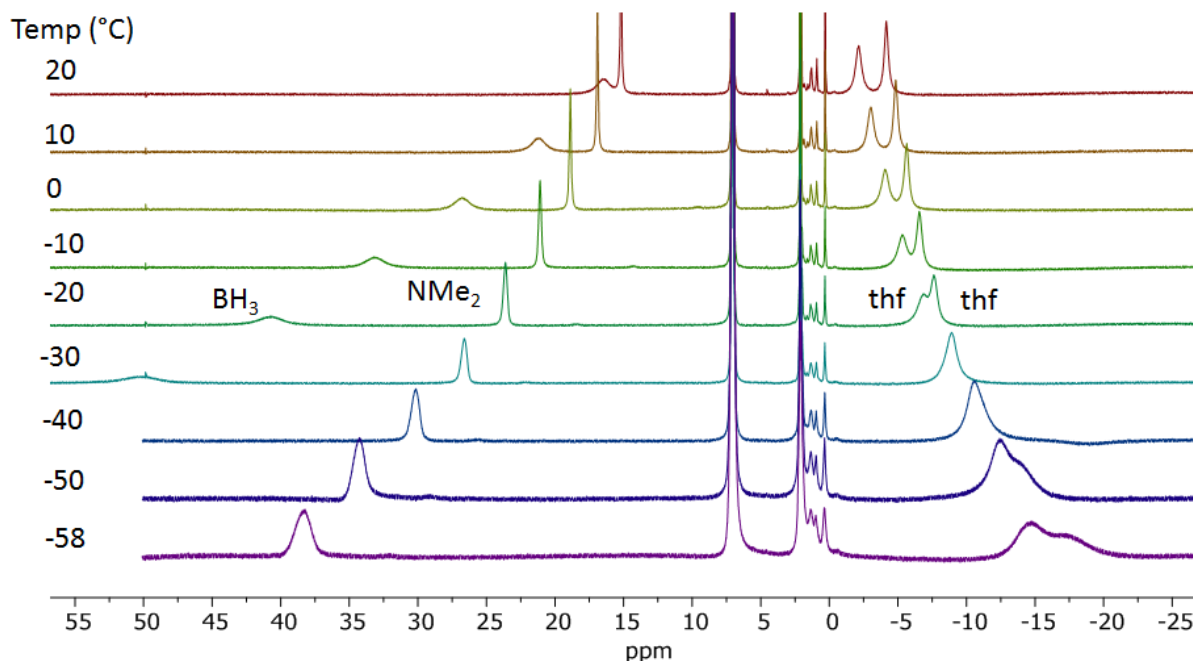
Figure 2.5. VT ^{1}H NMR spectra of the Tm(H$_3$BNMe$_2$BH$_3$)$_2$(thf)$_x$, **4/5**, in toluene-d_8.

adduct **4**, and association of thf to the bis thf adduct **5**, must be fast at this temperature. Here, comparing the ^{1}H-NMR spectrum of Tm(H$_3$BNMe$_2$BH$_3$)$_2$(thf)$_x$ with that of Tm(H$_3$BNMe$_2$BH$_3$)$_2$-(thf-d_8)$_x$ at 0 °C (Figure 2.4a) shows that the resonances at δ -4.03 and -5.60 can be assigned to thf. The remaining two peaks at δ 26.15 and 18.58 can then be assigned to the BH$_3$ and NMe$_2$ groups respectively, on the assumption that the broader of the two peaks should be due to the BH$_3$ protons, which are closer to the paramagnetic lanthanide center. The variable temperature ^{1}H NMR spectra of **4/5** is shown in Figure 2.5. Interestingly, the δ$_{dia}$ values of -146.6 (BH$_3$), -49.0 (NMe$_2$), 17.9 (thf), and 28.2 (thf) predicted by the y-intercepts of the Curie plots (Figure 2.6) of **4/5** are also inconsistent with the expected diamagnetic NMR shifts, and again suggest that TIP effects are present.

As with **1**, all the signals in the ^{1}H-NMR spectrum disappear when the spectrum is collected in thf-d_8, however, in the case of **4** and **5**, no new signals appear. Likewise, the ^{11}B-NMR spectrum
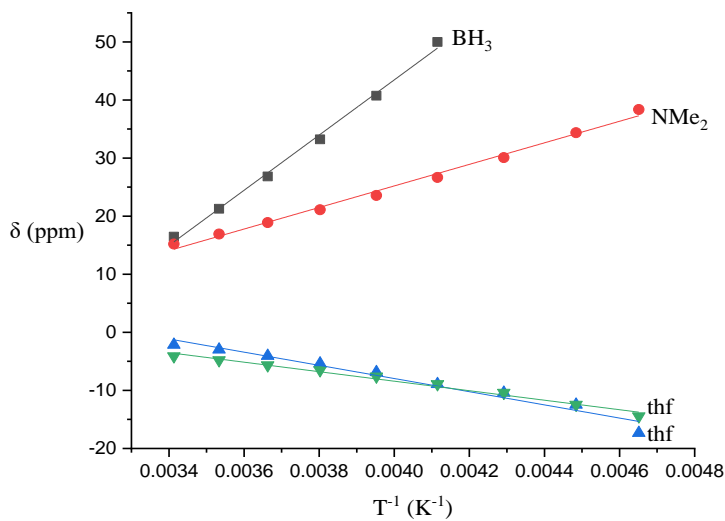
Figure 2.6. Curie plots for the VT-NMR experiment of **4/5**.

of **4** and **5** shifts from δ 4.8 in toluene-d_8 to δ 50 in thf-d_8, indicating that the presence of excess

thf converts **4** and **5** to a different species in solution.

The ^{1}H-NMR spectrum of $Sm(H_3BNMe_2BH_3)_2(dme)_2$, **2**, in toluene-$d_8$ contains three

singlets at δ 0.03, 0.15, and 5.23 with integration ratios of 1 : 1 : 2 (Figure 2.7). The former and

latter signals can be assigned to the methylene and methyl protons of the dme groups, respectively,

on the basis of their larger full width at half maximum (fwhm) values. Their broadness is a result

of more efficient relaxation promoted by their proximity to the paramagnetic center. The ^{11}B NMR

spectrum of **2** consists of a single broad resonance at δ 217.

No NMR spectra of $Sm(H_3BNMe_2BH_3)_2$(18-crown-6), **3**, could be obtained due to the

insolubility of this compound in toluene and other non-reactive solvents.

The IR spectra of **1-5** all contain bands between 2000 and 2500 cm^{-1} that correspond to the

B-H stretching modes of the DMADB ligand. Stretching bands at higher frequencies, namely

those at 2397, 2391, 2349, and 2359 cm^{-1}, in the IR spectrum of **1-5**, can be assigned to terminal
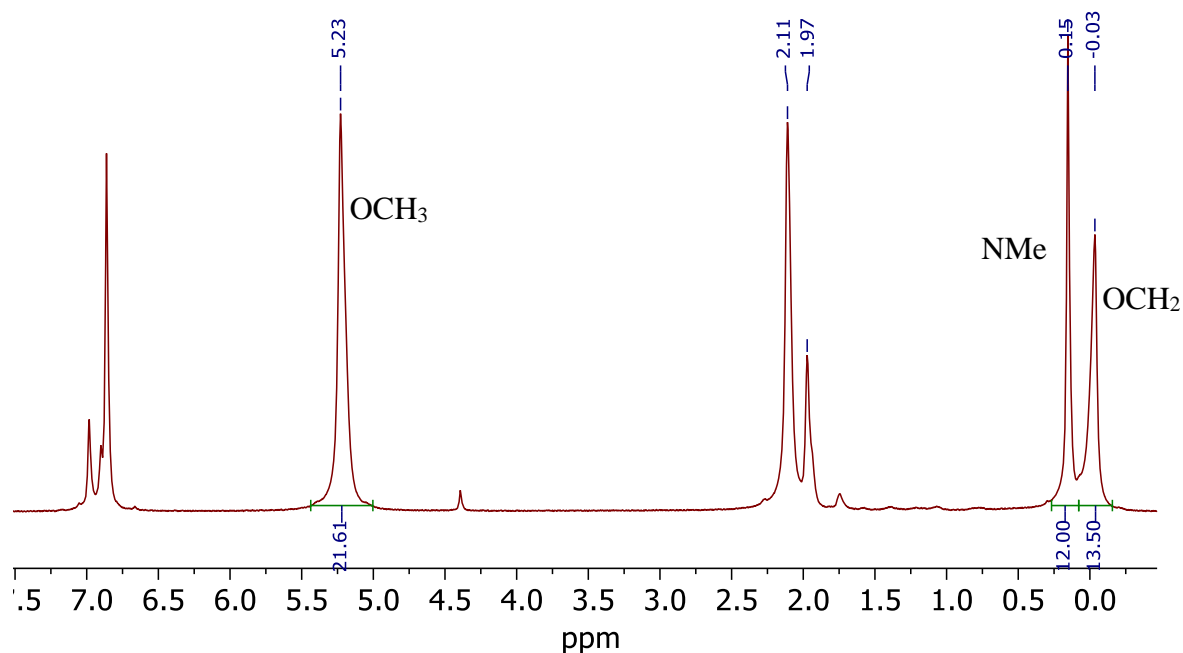
Figure 2.7. ^{1}H-NMR spectrum of **2** with integration values.

B-H stretching modes whereas bands at 2298 and 2250, 2296, 2252, and 2072, 2292, 2224, and 2066, 2295, 2226, and 2076 cm^{-1} can be assigned to metal-bound B-H stretches. These assignments are consistent with the IR spectra of other DMADB[27, 32, 36-41] and borohydride complexes.[42] It is worth noting, however, that the bands in this region are broad and the peaks are poorly resolved, which is probably a result of the weak covalent interaction between the lanthanide center and the DMADB ligand.

IR bands at 1034 and 879 cm^{-1} for complex **1** and at 1021 and 877 cm^{-1} for complex **4/5** can be assigned as C-O-C asymmetric stretches of the thf ligands.[27, 36, 43] Similarly, IR bands at 1106 and 853 cm^{-1} in the IR spectrum of **2** can be assigned to the C-O-C stretches of dme.[44, 45]

Crystal Structures of the New Complexes. The molecular structures of complexes **1-5** have been determined by X-ray crystallography (see Experimental Section for details). The coordination geometry of the samarium(II) complex Sm(H$_3$BNMe$_2$BH$_3$)$_2$(thf)$_3$, **1**, (Figure 2.8) is best described in terms of a distorted pentagonal bipyramid in which the four boron atoms of the

DMADB ligands occupy the equatorial sites along with one of the thf ligands; the other two thf ligands occupy the axial sites. Interestingly, although **1** is a monomer, the DMADB complex of the similarly sized europium(II) ion is not; rather, it is a dimer, $[Eu(H_3BNMe_2BH_3)_2(thf)_2]_2$.[27] The coordination spheres of the Eu centers in this molecule are also pentagonal bipyramids, but consist of two thf molecules, one chelating DMADB ligand, and three BH_3 groups from two bridging DMADB ligands.

The O2-Sm1-O3 bond angle of 163° involving the two axial oxygen atoms in **1** deviates slightly from the ideal value of 180° (Table 2.1); in the same manner, the apical oxygen atoms describe O-Sm1-B angles of 88-102° and O-Sm1-O1 angles of 79-85° to the equatorial groups, vs.
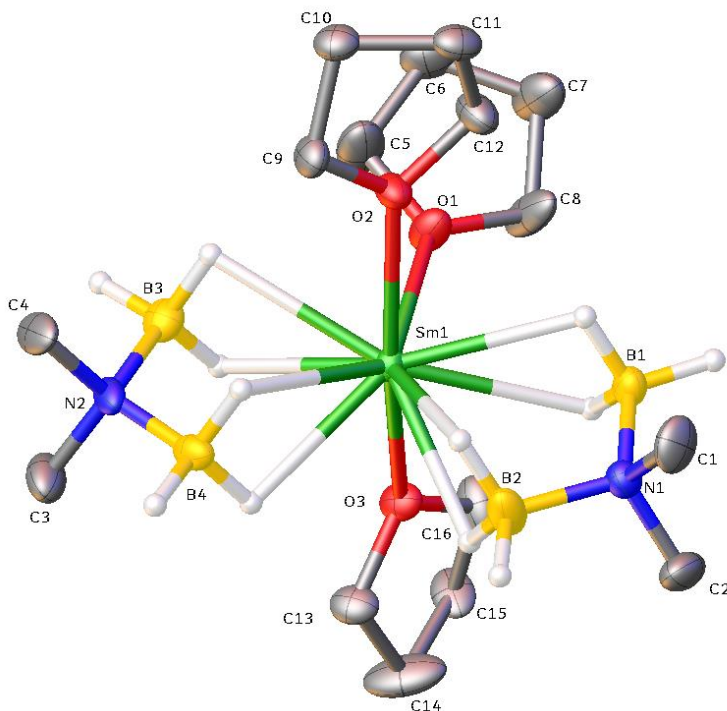
Figure 2.8. Molecular structure of $Sm(H_3BNMe_2BH_3)_2(thf)_3$, **1**. Ellipsoids show the 50% probability density surfaces. Hydrogen atoms attached to carbon and disordered components have been deleted for clarity.

the ideal value of 90°.

The Sm1-O2 and Sm1-O3 bond lengths to the axial oxygen atoms in **1** of 2.603 and 2.633 Å, respectively, are both slightly longer than the equatorial Sm1-O1 bond length of 2.545 Å. These distances are similar to those reported for other Sm^{II} thf compounds such as $[Sm(BH_4)_2(thf)_2]_n$,[46] $[Cp*Sm(BH4)(thf)_2]_2$,[46] $Sm[N(SiMe_3)]_2(thf)_2$,[47] and $[Cp*SmI(thf)_2]_2$.[48]

Two of the three hydrogen atoms on each boron in the DMADB ligands coordinate to the

Table 2.1. Selected bond lengths and angles for $Sm(H_3BNMe_2BH_3)_2(thf)_3$ (**1**).

Bond Lengths (Å)			
Sm1-O1	2.545 (5)	Sm1-H11	2.69 (2)
Sm1-O2	2.603 (5)	Sm1-H12	2.67 (2)
Sm1-O3	2.633 (5)	Sm1-H21	2.58 (2)
Sm1-B1	3.075 (8)	Sm1-H22	2.48 (2)
Sm1-B2	2.952 (8)	Sm1-H31	2.69 (2)
Sm1-B3	3.024 (8)	Sm1-H32	2.60 (2)
Sm1-B4	2.993 (8)	Sm1-H41	2.62 (2)
		Sm1-H42	2.56 (2)

Bond Angles (deg)			
O1-Sm1-O2	79.0 (2)	O3-Sm1-B2	90.2 (2)
O1-Sm1-O3	84.1 (2)	O3-Sm1-B3	89.2 (2)
O1-Sm1-B1	87.0 (2)	O3-Sm1-B4	96.2 (2)
O1-Sm1-B2	138.2 (2)	B1-Sm1-B2	51.4 (2)
O1-Sm1-B3	83.5 (2)	B1-Sm1-B3	170.4 (2)
O1-Sm1-B4	135.3 (2)	B1-Sm1-B4	137.7 (2)
O2-Sm1-O3	163.1 (2)	B2-Sm1-B3	138.0 (2)
O2-Sm1-B1	89.6 (2)	B2-Sm1-B4	86.5 (2)
O2-Sm1-B2	102.0 (2)	B3-Sm1-B4	51.9 (2)
O2-Sm1-B3	89.6 (2)	B1-N1-B2	111.7 (6)
O2-Sm1-B4	96.3 (2)	B3-N2-B4	111.9 (5)
O3-Sm1-B1	88.8 (2)		

metal center; the third hydrogen atom is terminal on boron. Thus, the Sm center in **1** can also be described as being 11 coordinate: there are 8 Sm-H bonds and 3 Sm-O bonds. The κ^2 Sm1-B distances, which range from 2.9-3.1 Å, are comparable to the bridging Sm-B bond distances of 2.931(5) and 2.91(1) Å observed for$[Sm(BH_4)_2(thf)_2]_n$ and $[Cp^*Sm(\mu\text{-}BH_4)(thf)_2]_2$ respectively[46]and the κ^2 Sm-B bond distances of 2.78-2.87 Å in $Sm(H_3BNMe_2BH_3)_3(thf)$.[32] The κ^2 Sm1-B bond distances are comparable to the κ^2 Eu1-B distances of 2.88-3.13 Å reported for $Eu(H_3BNMe_2BH_3)_2(thf)$.[27] Likewise, the Sm1-H distances of 2.48-2.7 Å are also comparable to those reported for the Eu^{II} complex; these similarities are no doubt due to the fact that Eu and Sm are neighboring elements in the lanthanide series and thus have very similar radii in the same oxidation state.
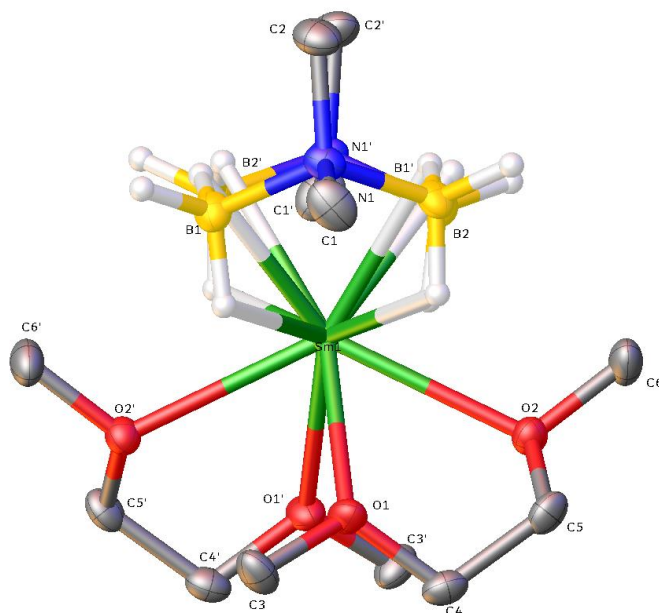
Figure 2.9. Molecular structure of $Sm(H_3BNMe_2BH_3)_2(dme)_2$ (**2**) viewed along the pseudo-threefold axis of the distorted trigonal prism. Ellipsoids show the 50% probability density surfaces. Hydrogen atoms attached to carbon and disordered components have been deleted for clarity.

31

Table 2.2. Selected bond lengths and angles for $Sm(H_3BNMe_2BH_3)_2(dme)_2$ (**2**).

Bond Lengths (Å)			
Sm1-O1	2.660 (3)	Sm1-H11	2.76 (2)
Sm1-O2	2.658 (3)	Sm1-H12	2.62 (2)
Sm1-B1	3.074 (5)	Sm1-H21	2.66 (2)
Sm1-B2	3.056 (6)	Sm1-H22	2.64 (2)

Bond Angles (deg)			
O1-Sm1-O2	62.4 (1)	O2-Sm1-B2	79.2 (1)
O1-Sm1-O1′	76.5 (1)	O2-Sm1-B1′	82.7 (1)
O1-Sm1-O2′	77.2 (1)	O2-Sm1-B2′	131.2 (1)
O1-Sm1-B1	87.8 (1)	B1-Sm1-B2	50.6 (1)
O1-Sm1-B2	50.6 (1)	B1-Sm1-B1′	121.2 (2)
O1-Sm1-B1′	144.0 (1)	B1-Sm1-B2′	96.0 (1)
O1-Sm1-B2'	155.4 (1)	B2-Sm1-B2′	114.6 (2)
O2-Sm1-O2′	128.3 (1)	B1-N1-B2	111.0 (3)
O2-Sm1-B1	123.8 (1)		

Molecules of the dme complex $Sm(H_3BNMe_2BH_3)_2(dme)_2$, **2**, lie on a crystallographic two-fold axis (Figure 2.9); atoms that are related by this symmetry element are denoted with primes. The coordination geometry about the metal atom in **2** is best described in terms of a bi-capped trigonal prism in which O2 and O2′ are the capping ligands, and the planes formed by B1, B2, and O1, and by B1′, B2′, and O2′, are the triangular faces. These two planes deviate slightly from parallel and form a dihedral angle of 19.6°. The bicapped trigonal prismatic geometry is shared by $Eu(H_3BNMe_2BH_3)_2(dme)_2$ which, unlike its thf analog, exists in the solid state as a monomer and is isostructural with **2**. The Sm center in **2** can also be described as being 12 coordinate (8 Sm-H bonds and 4 Sm-O bonds).

The Sm1-O bond lengths of 2.658 and 2.660 Å are also similar to those observed in **1** and other Sm^{II} complexes.[29] The Sm-B distances of 3.074 and 3.056 Å and Sm-H distances of 2.66 to 2.76 Å (Table 2.2) are similar to those observed in **1**.

Several authors have commented that complexes of divalent lanthanides often resemble those of the larger alkaline earth metals,[49, 50] and the structures of **1** and **2** are no exception: both are isostructural with their respective Sr analogs, $Sr(H_3BNMe_2BH_3)_2(thf)_3$ and $Sr(H_3BNMe_2BH_3)_2(dme)_2$.[36] These similarities reflect the similarities in the charge and sizes of Sr^{II} (r_{ionic} = 1.35 Å) vs. Sm^{II} (r_{ionic} = 1.36 Å).[51]

The structure of the crown ether complex $Sm(H_3BNMe_2BH_3)_2(18\text{-crown-}6)$, **3**, (Figure 2.10) is best described as a polyhedron of idealized C_{2v} symmetry consisting of a planar hexagonal girdle capped on one side by a single vertex and the other side by a pair of vertices.[37] In **3**, the six oxygen atoms act as the hexagonal girdle, whereas B1 occupies the single capping vertex and B3 and B4 occupy the pair of capping vertices. The coordination number of the Sm center can be described either as 9 coordinate (three Sm-B bonds and six Sm-O bonds) or 12 coordinate (six Sm-H bonds and six Sm-O bonds).

The Sm1A-O bond lengths in **3** of 2.68 to 2.77 Å (Table 2.3) are slightly longer than those in Sm^{III} 18-crown-6 complexes as expected,[52] but are consistent with those reported for other Sm^{II} 18-crown-6 complexes.[53-55] Three of the Sm1A-B distances lie between 3.08 and 3.19 Å, and the Sm1A-H distances involving those boron atoms are 2.6-2.9 Å. In contrast, the Sm1A-B4 distance is 4.533 Å and the Sm1A-H distances to this boron atom are all greater than 4 Å; all of these distances clearly indicate that B4 is not bonded to the metal center.

Interestingly, **3** is the first divalent DMADB complex bearing a crown ether ligand in which

the DMADB ligand is bound to the metal. The other three complexes, [Ca(12-crown-4)$_2$]-[H$_3$BNMe$_2$BH$_3$]$_2$, [Sr(12-crown-4)$_2$][H$_3$BNMe$_2$BH$_3$]$_2$,[36] and [Ba(18-crown-6)$_2$][H$_3$BNMe$_2$BH$_3$]$_2$[37] all exist as the purely ionic species.
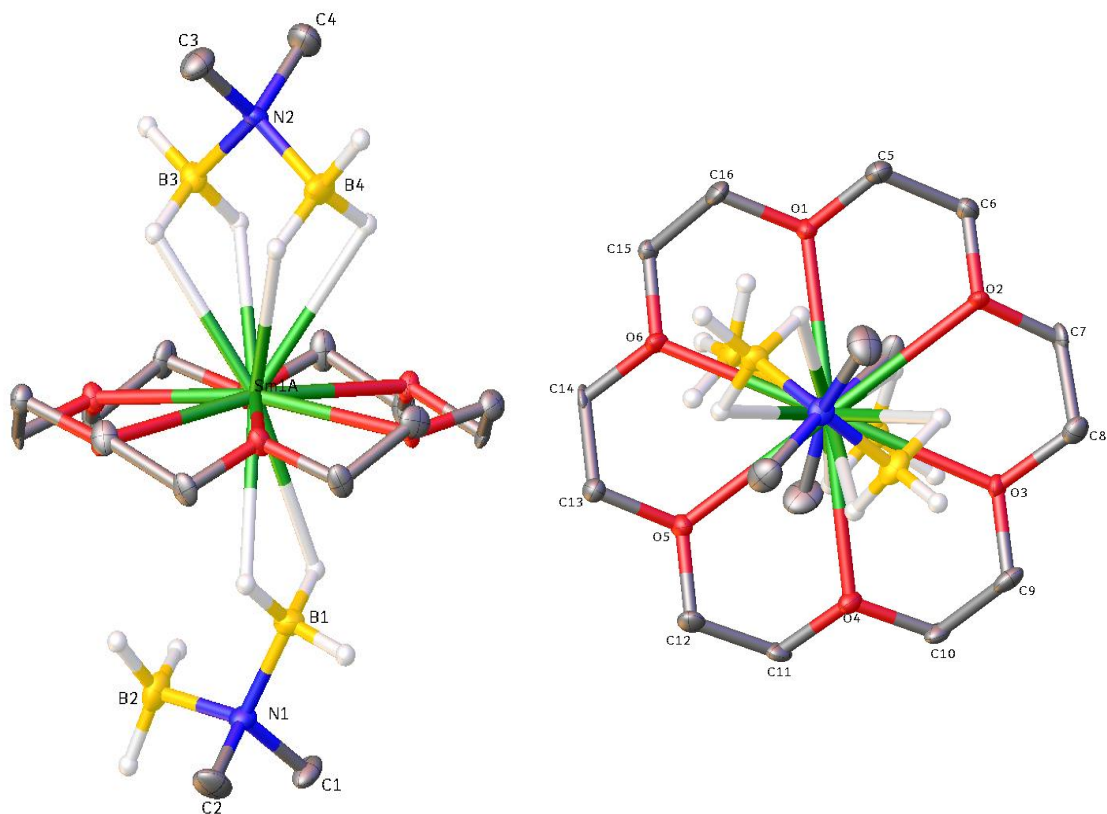
Figure 2.10. Two views of the molecular structure of Sm(H$_3$BNMe$_2$BH$_3$)$_2$(18-crown-6) (**3**). Ellipsoids indicate the 50% probability density surfaces. Hydrogen atoms attached to carbon and disordered components have been deleted for clarity.

For thulium, we have isolated and characterized a co-crystal consisting of equal numbers of the tris thf complex Tm(H$_3$BNMe$_2$BH$_3$)$_2$(thf)$_3$, **4**, and the bis thf complex Tm(H$_3$BNMe$_2$BH$_3$)$_2$(thf)$_2$, **5**. Compound **4** (Figure 2.11) is isostructural with the samarium tris thf

Table 2.3. Selected bond lengths and angles for $Sm(H_3BNMe_2BH_3)_2$(18-crown-6) (**3**).

Bond Lengths (Å)			
Sm1A-O1	2.747 (3)	Sm1A-B4	3.197 (4)
Sm1A-O2	2.741 (3)	Sm1A-H11	2.67 (2)
Sm1A-O3	2.683 (2)	Sm1A-H13	2.61 (2)
Sm1A-O4	2.773 (3)	Sm1A-H21	4.00 (2)
Sm1A-O5	2.748 (3)	Sm1A-H23	4.42 (2)
Sm1A-O6	2.742 (2)	Sm1A-H31	2.56 (2)
Sm1A-B1	3.086 (4)	Sm1A-H32	2.64 (2)
Sm1A-B2	4.533 (4)	Sm1A-H41	2.90 (2)
Sm1A-B3	3.091 (4)	Sm1A-H42	2.65 (2)

Bond Angles (deg)			
O1-Sm1A-O2	60.06 (8)	B1-Sm1A-B2	34.8 (1)
O1-Sm1A-O3	119.0 (1)	B1-Sm1A-B3	166.6 (1)
O1-Sm1A-O4	167.4 (1)	B1-Sm1A-B4	144.5 (1)
O1-Sm1A-O5	117.59 (8)	B2-Sm1A-B3	132.3 (1)
O1-Sm1A-O6	60.00 (8)	B2-Sm1A-B4	176.814
O1-Sm1A-B1	88.47 (9)	B3-Sm1A-B4	48.604
O1-Sm1A-B2	68.588	B1-N1-B2	112.6 (3)
O1-Sm1A-B3	80.40 (9)	B3-N2-B4	110.2 (3)
O1-Sm1A-B4	114.374		

complex **1**. It adopts a similar pentagonal bipyramidal geometry in which O1 and O2 reside in the axial position, and the boron atoms, along with O3, reside in the equatorial positions. The O1-Tm1-O2 bond angle of 172° (Table 2.4) deviates only slightly from linearity; likewise, the O-Tm-B bond angles to the apical oxygen atoms lie in the range of 87 to 95° and O-Tm-O3 bond angles of 86° are all close to 90°.

The axial Tm-O bond lengths of 2.462 and 2.471 Å are slightly longer than the equatorial Tm-O bond length of 2.496 Å. All three Tm-O bond lengths are considerably shorter than those seen in **1**, as are the Tm-B distances of 2.89 to 2.93 Å and the Tm-H bond distances of 2.49-2.61

Å. The shorter bond lengths observed in **4** reflect the smaller ionic radius of thulium vs. samarium.

The structure of the bis thf complex $Tm(H_3BNMe_2BH_3)_2(thf)_2$, **5**, (Figure 2.11) is best considered as a distorted cis-octahedron because there are exactly three large inter-ligand bond angles: O4-Tm2-B5 = 140.5°, O5-Tm2-B8 = 139.5°, and B6-Tm2-B7 = 157.2° (Table 2.4). The Tm-O bond lengths of 2.391 and 2.398 Å, the Tm-B bond lengths of 2.801 and 2.843 Å, and the Tm-H bond lengths of 2.39 to 2.51 Å are all slightly shorter than those observed for the tris thf adduct **4**; the shorter bond distances in **5** reflect the smaller steric crowding around the Tm center due to the lower coordination number.
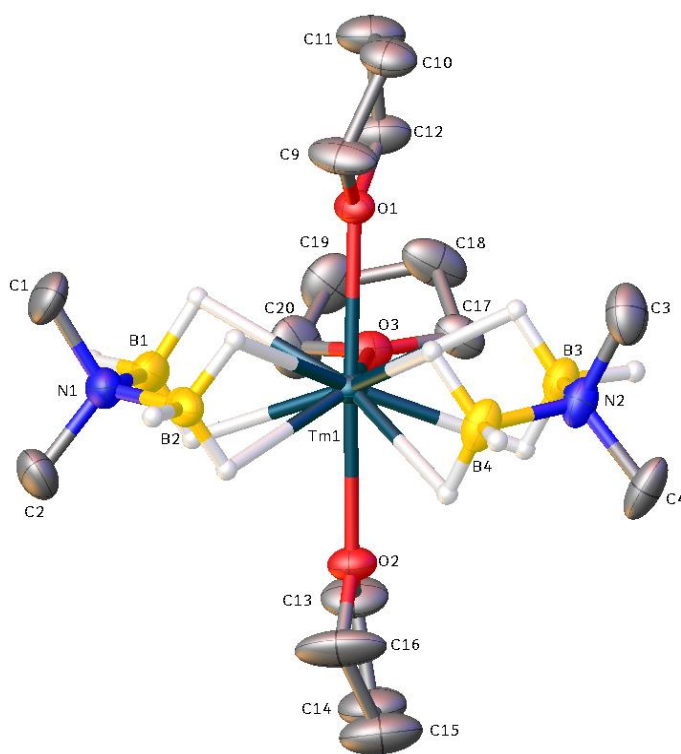
Figure 2.11. Molecular structure of $Tm(H_3BNMe_2BH_3)_2(thf)_3$ (**4**). Ellipsoids show the 50% probability density surfaces. Hydrogen atoms attached to carbon and disordered components have been deleted for clarity.
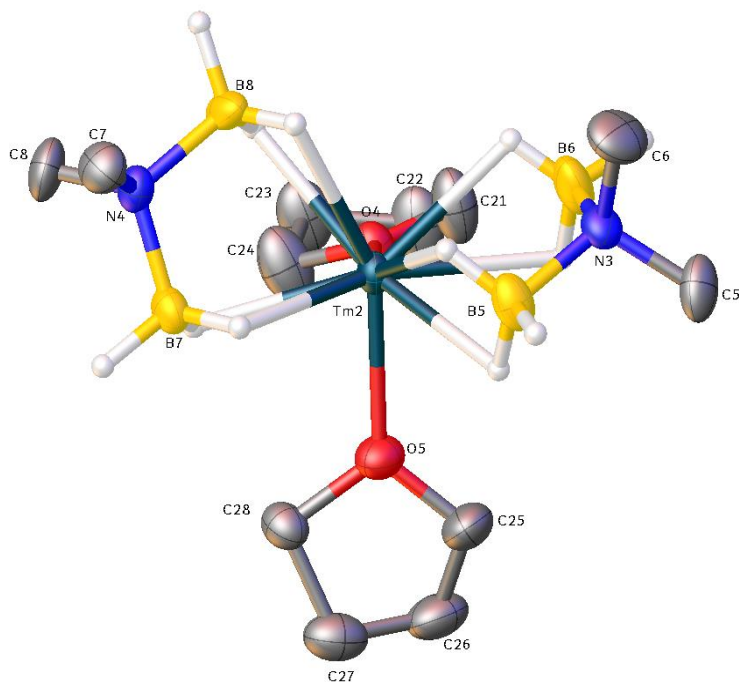
Figure 2.12. Molecular structure of $Tm(H_3BNMe_2BH_3)_2(thf)_2$, **5**. Ellipsoids show the 50% probability density surfaces. Hydrogen atoms attached to carbon and disordered components have been deleted for clarity.

Structurally similar to **5** are the Yb^{II} and Ca DMADB analogs $Yb(H_3BNMe_2BH_3)_2(thf)_2$[27] and $Ca(H_3BNMe_2BH_3)_2(thf)_2$,[36] which also adopt cis octahedral geometries. Because Tm and Yb are neighbors in the lanthanide series, they have similar radii in the same oxidation state, and as a result the M-O, M-B, and M-H bond lengths in $Yb(H_3BNMe_2BH_3)_2(thf)_2$ are similar to those in **5**. The Tm-O and Tm-H bond distances in **4** and **5** are also both comparable to those seen for other Tm^{II} complexes.[5, 50] The Tm-B distances are not so comparable, however, because they depend on the number of hydrogen atoms that bridge between boron and the metal atom.[56]

Volatility Studies of 1. Unlike their trivalent analogues, the divalent compounds **1-5** do not sublime at 100 °C in vacuum (1 Torr); instead they decompose when heated under these conditions.[11] This limited volatility, which has also been observed for the Eu^{II}, Yb^{II}, and the

37

isostructural Sr bis-DMADB analogs, has been attributed to de-solvation during heating.[27, 36] Analogous studies of alkaline earth metal β-diketonates and pyrazolylborates bearing ether ligands have shown that these complexes tend to desolvate upon heating, and other studies suggest that after de-solvation these complexes oligomerize to form non-volatile species.[49, 57-59] Taken together, these examples suggest that desolvation followed by oligomerization likely plays a role in the low volatility of **1**.

Table 2.4. Selected bond lengths and angles for $Tm(H_3BNMe_2BH_3)_2(thf)_3$ (**4**).

Bond Lengths (Å)			
Tm1-O1	2.462 (3)	Tm1-H11	2.54 (5)
Tm1-O2	2.471 (4)	Tm1-H12	2.57 (6)
Tm1-O3	2.496 (4)	Tm1-H21	2.49 (5)
Tm1-B1	2.910 (7)	Tm1-H22	2.49 (6)
Tm1-B2	2.894 (6)	Tm1-H31	2.61 (6)
Tm1-B3	2.927 (6)	Tm1-H32	2.52 (6)
Tm1-B4	2.912 (7)	Tm1-H41	2.58 (6)
		Tm1-H42	2.53 (6)

Bond Angles (deg)			
O1-Tm1-O2	172.3 (1)	O3-Tm1-B2	133.3 (2)
O1-Tm1-O3	86.5 (1)	O3-Tm1-B3	81.5 (2)
O1-Tm1-B1	89.6 (2)	O3-Tm1-B4	135.2 (2)
O1-Tm1-B2	91.5 (2)	B1-Tm1-B2	53.9 (2)
O1-Tm1-B3	87.2 (2)	B1-Tm1-B3	160.8 (2)
O1-Tm1-B4	93.2 (2)	B1-Tm1-B4	145.4 (2)
O2-Tm1-O3	85.9 (1)	B2-Tm1-B3	145.0 (2)
O2-Tm1-B1	90.1 (2)	B2-Tm1-B4	91.5 (2)
O2-Tm1-B2	94.5 (2)	B3-Tm1-B4	53.8 (2)
O2-Tm1-B3	90.6 (2)	B1-N1-B2	111.6 (5)
O2-Tm1-B4	91.5 (2)	B3-N2-B4	110.9 (4)
O3-Tm1-B1	79.4 (2)		

Table 2.5. Selected bond lengths and angles for $Tm(H_3BNMe_2BH_3)_2(thf)_2$ (**5**).

Bond Lengths (Å)			
Tm2-O4	2.392 (4)	Tm2-H52	2.40 (6)
Tm2-O5	2.398 (4)	Tm2-H61	2.42 (7)
Tm2-B5	2.834 (7)	Tm2-H62	2.51 (6)
Tm2-B6	2.825 (7)	Tm2-H71	2.39 (7)
Tm2-B7	2.801 (6)	Tm2-H72	2.45 (7)
Tm2-B8	2.843 (6)	Tm2-H81	2.44 (7)
Tm2-H51	2.44 (6)	Tm2-H82	2.49 (7)

Bond Angles (deg)			
O4-Tm2-O5	81.4 (1)	B5-Tm2-B6	55.5 (2)
O4-Tm2-B5	140.5 (2)	B5-Tm2-B7	111.2 (2)
O4-Tm2-B6	89.0 (2)	B5-Tm2-B8	111.1 (2)
O4-Tm2-B7	107.9 (2)	B6-Tm2-B7	157.2 (3)
O4-Tm2-B8	95.8 (2)	B6-Tm2-B8	109.4 (3)
O5-Tm2-B5	94.8 (2)	B7-Tm2-B8	54.9 (2)
O5-Tm2-B6	111.0 (2)	B5-N3-B6	111.8 (5)
O5-Tm2-B7	87.3 (2)	B7-N4-B8	110.7 (4)
O5-Tm2-B8	139.5 (2)		

Experimental Section

All operations were carried out in a vacuum or under argon using standard Schlenk techniques. All glassware was dried in an oven at 150 °C, assembled hot, and allowed to cool under a vacuum before use. Tetrahydrofuran (thf), diethyl ether (Et$_2$O), and pentane were distilled under nitrogen from sodium/benzophenone, and 1,2-dimethoxyethane (dme) was distilled under nitrogen from calcium hydride before use. Sm powder (40 mesh, Thermo Fisher Scientific Chemical), Tm powder (40 mesh, Strem), I$_2$ (Sigma), and 1,2-diiodoethane (Alfa Aesar) were used as received. Na(H$_3$BNMe$_2$BH$_3$),[60] Sm(H$_3$BNMe$_2$BH$_3$)$_3$(thf),[32] SmI$_2$(thf)$_2$,[28] and solutions of TmI$_2$

in thf[8] were prepared in accordance with the literature. The concentration of TmI_2 was approximated by using a known volume of thf and assuming complete conversion of I_2 to TmI_2.

Elemental analyses were carried out by the University of Illinois Microanalytical Laboaratory. The IR spectra were recorded on a Nicolet 200 infrared spectrometer as Nujol mulls between KBr plates. The ^1H NMR data were obtained on a Varian Unity Inova 400 instrument at 400 MHz, Varian Unity U500 instrument at 500 MHz or a Varian VXR 500 instrument at 500 MHz. The ^{11}B NMR data were obtained on a Varian Unity Inova 400 instrument at 128 MHz. Chemical shifts are reported in δ units (positive shifts to high frequency) relative to tetramethylsilane (^1H NMR) or $BF_3 \cdot Et_2O$ (^{11}B NMR). Melting points were determined in closed capillaries under argon on a Thomas-Hoover Unimelt apparatus

Bis(*N*,*N*-dimethylaminodiboranato)tris(tetrahydrofuran)samarium(II),

$Sm(H_3BNMe_2BH_3)_2(thf)_3$ (1). Method A. To a dark blue solution of $SmI_2(thf)_2$ (0.96 g, 1.75 mol) in thf (30 mL) was added a solution of $Na(H_3BNMe_2BH_3)$ (0.33 g, 3.5 mmol) in thf (30 mL). This mixture was stirred for 24 h at room temperature. The tetrahydrofuran was removed in vacuum to yield a reddish-purple residue, which was extracted with pentane (2×50 mL). The dark purple extracts were filtered, combined, concentrated to ca. 20 mL, and cooled to -20 °C to give dark purple cubes. Yield: 0.31 g (34 %). Mp: 94-98 °C. Anal. Calcd for $C_{16}H_{48}B_4N_2O_3Sm$: C, 37.7; H, 9.48; N, 5.49. Found: C, 34.6; H, 9.31; N, 5.79. IR (cm^{-1}): 2397 w, 2298 m, 2250 m, 1225 w, 1208 w, 1174 sh, 1146 sh, 1090 br, 1034 m, 923 w, 879 w, 799 m, 723 w. ^1H NMR (C_7D_8, 10 °C): δ 0.16 (s, fwhm = 19 Hz, CH_2, 12 H), 2.71 (s, fwhm = 26 Hz, NMe_2, 12 H), 3.14 (s, fwhm = 46 Hz, CH_2, 12 H). ^{11}B NMR (C_7D_8, 20 °C): δ -259.5 (br s, fwhm = 350 Hz, BH_3).

Method B. To a suspension of KC_8 (0.082 g, 0.61 mol) in thf (20 mL) was added a pale-yellow solution of $Sm(H_3BNMe_2BH_3)_3(thf)$ (0.26 g, 0.62 mmol) in thf (20 mL), at which point the

solution color immediately turned cherry red. This mixture was stirred for 24 h at room temperature and then filtered to yield a dark red solution. This solution was concentrated in vacuum to ca. 5 mL. Pentane (5 mL) was layered on top of this solution and the mixture was cooled overnight at -20 °C to yield an equal mixture of dark red needles and a few white needles presumed to be $K(H_3BNMe_2BH_3)$. XRD analysis of the red crystals from the first crystallization showed that they have a unit cell identical to that of $Sm(H_3BNMe_2BH_3)_2(thf)_3$.

Bis(*N,N*-dimethylaminodiboranato)bis(1,2-dimethoxyethane)samarium(II),

Sm(H₃BNMe₂BH₃)₂(dme)₂ (2). A bright red solution of $Sm(H_3BNMe_2BH_3)_2(thf)_3$ (0.25 g, 0.49 mmol) in 1,2-dimethoxyethane (9.0 mL, 7.8 g, 87 mmol) was stirred for 2 h and concentrated to ca. 2 mL in vacuum. Pentane (2 mL) was layered on top of the solution, and the mixture was cooled overnight at -20 °C to yield dark red needles. Yield: 0.076 g (33%). M.p.: 96-104 °C (dec.). Anal. Calcd for $C_{12}H_{44}B_4N_2O_4Sm$: C, 30.4; H, 9.35; N, 5.91. Found: C, 30.3; H, 9.52; N, 6.03. IR (cm^{-1}): 2391 b, 2296 s, 2252 s, 2072 m, 1304 m, 1223 s, 1178 s, 1152 s, 1106 s, 1061 s, 1017 s, 979 s, 926 s, 905 m, 853 s, 801 s, 738 w, 685 w. ^{1}H NMR (C$_7$D$_8$, 20 °C): δ 0.03 (s, fwhm = 19.5 Hz, 12 H, OCH$_2$), 0.15 (s, fwhm = 8.06, 12 H, NMe$_2$), 5.23 (s, fwhm = 22 Hz, 22 H, OMe). ^{11}B NMR (C$_7$D$_8$, 20 °C): δ -217.7 (br s, fwhm = 250 Hz, BH$_3$).

Bis(*N,N*-dimethylaminodiboranato)(18-crown-6)samarium(II), Sm(H₃BNMe₂BH₃)₂-(18-crown-6) (3) To a suspension of KC$_8$ (0.075 g, 0.56 mmol) and 18-crown-6 (0.156 g, 0.59 mmol) in Et$_2$O (10 mL) was added a pale-yellow solution of $Sm(H_3BNMe_2BH_3)_3(thf)$ (0.28 g, 0.54 mmol) in Et$_2$O (20 mL). The mixture was stirred for 2 h at room temperature, at which point a black precipitate slowly began to form. After 2 h, this Et$_2$O solution was decanted and discarded. Compound **3** was extracted from the black precipitate with thf (2 × 10 mL). The red extracts were filtered, combined, and dried in vacuum to afford a pink solid. Yield: 0.070 g (23%). X-ray quality

crystals of **3** were grown by vapor diffusion of Et_2O into the red extracts. Compound **3** has limited solubility in thf; once dry, it will not go back into solution. M.p.: >250 °C Anal. Calcd for $C_{16}H_{48}B_2N_2O_6Sm$: C, 34.4; H, 8.67; N, 5.02. Found: C, 36.1; H, 8.50; N, 5.00. IR (cm^{-1}): 2349 s, 2293 s, 2224 s, 2067 w, 1286 sh, 1153 sbr, 1093 sbr, 1016 s, 973 m, 920 w, 840 m, 799 br, 723 w.

Bis(*N,N*-dimethylaminodiboranato)tris(tetrahydrofuran)thulium(II), Tm(H$_3$BNMe$_2$-BH$_3$)$_2$(thf)$_3$ (4) and Bis(*N,N*-dimethylaminodiboranato)bis(tetrahydrofuran)thulium(II), Tm(H$_3$BNMe$_2$BH$_3$)$_2$(thf)$_2$ (5), 1:1 co-crystal. To a solution of Na(H$_3$BNMe$_2$BH$_3$) (0.39 g, 4.1 mmol) in thf (20 mL) was added a green solution of TmI$_2$(thf)$_x$ in thf (45 mL of a 0.044 M solution, 2.0 mmol). This solution was stirred for 24 h at room temperature. The tetrahydrofuran was removed in vacuum to yield a dark brown residue, which was extracted with pentane (2×50 mL). The dark brown extracts were filtered, combined, concentrated to ca. 25 mL, and cooled overnight at -20 °C to yield dark brown prisms. Yield: 0.42 g (43%). M.p.: 95-98°C Anal. Calcd for $C_{14}H_{44}B_4N_2O_{2.5}Tm$: C, 34.1; H, 9.00; N, 5.69. Found: C, 31.6; H, 8.96; N, 5.87. IR (cm^{-1}): 2359 s br, 2296 s br, 2227 s br, 2076 s, 1230 s, 1213 s, 1175 s, 1146 s, 1021 s, 927 s, 905 s, 877 s, 800 s, 724 m. ^{1}H NMR (C$_7$D$_8$, 0 °C): δ -5.70 (s, fwhm = 194 Hz, CH$_2$, 16 H), -4.05 (s, fwhm = 336 Hz, CH$_2$, 16 H), 18.85 (s, fwhm = 69 Hz, NMe$_2$, 12 H), 26.70 (br s, fwhm = 629 Hz, BH$_3$, 9 H). ^{11}B NMR (C$_7$D$_8$, 20 °C): δ 4.8 (br s, fwhm = 420 Hz, BH$_3$).

Crystallographic Studies. Single crystals of **1**, **2**, **3**, and the mixed crystal **4/5** were mounted on glass fibers with dried, degassed Nujol (**1**, **2**, and **3**) or Krytox oil (DuPont) (**4/5**) and immediately cooled to -173 °C (**1**, **2**, and **3**) or -75 °C (**4/5**) in a cold nitrogen gas stream on the diffractometer. Standard peak search and indexing procedures gave rough cell dimensions, and least squares refinement yielded the cell dimensions given in Table 2.6 and 2.7.

Data were collected with an area detector by using the measurement parameters listed in

Tables 2.6 and 2.7. The measured intensities were reduced to structure factor amplitudes and their estimated standard deviations by correction for background, scan speed, and Lorentz and polarization effects. For all crystals, no corrections for crystal decay were necessary, but a multi-scan correction was applied; the minimum and maximum transmission factors are recorded in Tables 2.6 and 2.7. Systematically absent reflections were deleted, and symmetry equivalent reflections were averaged to yield the set of unique data. Unless otherwise noted, all unique data were used in the least squares refinement.

For all crystals, the analytical approximations to the scattering factors were used, and all structure factors were corrected for both the real and imaginary components of anomalous dispersion. In the final cycle of least squares, independent anisotropic displacement factors were refined for the non-hydrogen atoms. Hydrogen atoms attached to carbon were placed in idealized positions with C-H (methyl) = 0.98 Å, and C-H (methylene) = 0.99 Å; the methyl groups were allowed to rotate about the C-X axis to find the best least-squares positions. The displacement parameters for methylene and borane hydrogen atoms were set equal to 1.2 times U_{eq} for the attached carbon; those for methyl hydrogens were set to 1.5 times U_{eq}.

Sm(H₃BNMe₂BH₃)₂(thf)₃, 1: The orthorhombic lattice and the systematic absences 0kl, k ≠ 2n, h0l, l ≠ 2n, and hk0, h ≠ 2n, were uniquely consistent with space group *Pbca*. The structure was solved by direct methods (SHELXTL). The correct position for the samarium atom was deduced from an E-map; subsequent least-squares refinement and difference Fourier calculations revealed the positions of the remaining non-hydrogen atoms. One carbon atom (C15) of one of the tetrahydrofuran rings was disordered; the atom was partitioned over two positions and the site occupancy factors (SOFs) of these positions were refined subject to the constraint that the sum of these SOFs was equal to one; the SOF for the major site refined to 0.56(3). The quantity minimized

43

by the least-squares program was $\Sigma w(F_o^2 - F_c^2)^2$, where $w = [\sigma(F_o^2)]^2 + 63.10P^{-1}$ and $P = (F_o^2 + 2F_c^2)/3$. Hydrogen atoms attached to boron were located in the difference maps and their positions were refined independently subject to the restraints that all the B-H distances, and all the gem H-H distances, were approximately equal to one another (SADI 0.001). An isotropic extinction parameter was refined to a final value of $x = 9.7(8) \times 10^{-7}$ where F_c is multiplied by the factor $k[1 + F_c^2 x\lambda^3/\sin 2\theta]^{-1/4}$ with k being the overall scale factor. Successful convergence was indicated by the maximum shift/error of 0.002 for the last cycle. Final refinement parameters are given in Table 1. The largest peak and deepest hole in the final Fourier difference map were 0.64 e$\mathring{A}^{-3}$ and -0.84 e$\mathring{A}^{-3}$, respectively; the former was located 1.00 $\mathring{A}$ from Sm1. A final analysis of variance between observed and calculated structure factors showed some dependence on amplitude (especially for the weakest data) but no dependence on resolution. Reflections hkl with k large and $I_{obs} > I_{calc}$ were overly represented in the "most disagreeable reflections" list.

Sm(H$_3$BNMe$_2$BH$_3$)$_2$(dme)$_2$, 2: The systematic absences hkl, $h+k \neq 2n$, and $00l$, $l \neq 2n$, were uniquely consistent with the space group $C222_1$. Three reflections (006, 022, and 110) were statistical outliers (blocked by the beam stop) and omitted; the remaining 5183 unique data were used in the least squares refinement. The structure was solved by intrinsic phasing (SHELXTL). Correct positions for all the non-hydrogen atoms except for C7 were deduced from an E-map. Subsequent least-squares refinement and difference Fourier calculations revealed the positions of C7. The quantity minimized by the least-squares program was $\Sigma w(F_o^2 - F_c^2)^2$, where $w = [\sigma(F_o^2)]^2 + (0.0260P)^2 + 15.00 \, P^{-1}$ and $P = (F_o^2 + 2F_c^2)/3$. Hydrogen atoms attached to boron were independently refined subject to the restraint that the B-H distances and gem H-H distances were approximately equal to one another (SADI 0.001). An isotropic extinction parameter was refined to a final value of $x = 1.3(1) \times 10^{-6}$ where F_c is multiplied by the factor $k[1 + F_c^2 x\lambda^3/\sin 2\theta]^{-1/4}$ with

k being the overall scale factor. Successful convergence was indicated by the maximum shift/error of 0.002 for the last cycle. Final refinement parameters are given in Table 1. The largest peak and deepest hole in the final Fourier difference map were 1.48 and -0.78 eÅ^{-3}, respectively, the former was located 1.58 Å from O4. A final analysis of variance between observed and calculated structure factors showed no apparent errors.

Sm(H₃BNMe₂BH₃)₂(18-crown-6), 3: The monoclinic lattice, systematic absences 0*k*0, *k* ≠ 2*n*, and the average values of the normalized structure factors suggested the space group $P2_1$, which was confirmed by the success of the subsequent refinement. Systematically absent reflections were deleted and symmetry equivalent reflections were averaged to yield the set of unique data. The reflections (-3 3 9), (1 2 1), (1 -2 1), (-3 -3 9), (1 9 7), (0 2 0), (0 -2 0), (-1 3 3), (-2 -3 4), (-1 2 3), (-2 -2 2), (-1 4 1), (2 6 2), (-3 1 1), (-8 14 6), (-1 -2 3), (-3 -1 1), (3 2 5), (2 -2 2), (4 -1 2), (0 -6 0), (-1 -4 5), (0 -8 0), (2 -3 0), (2 -1 4), (0 6 0), (3 -1 3), (0 8 0), and (2 1 4) were omitted. During the collection of this data set the beam stop was positioned incorrectly, and these reflections (most of which have *hkl* indices that would not typically be considered as beam stop reflections) were inadvertently obscured by the edge of the bar that connects the circular beam stop to the instrument. The remaining 16143 unique data were used in the least squares refinement. The structure was solved by Patterson methods (SHELXTL). Initial positions for Sm1 and Sm2 were deduced from a Patterson map. Subsequent least-squares refinement and difference Fourier calculations revealed the positions of the remaining non-hydrogen atoms. The quantity minimized by the least-squares program was $\Sigma w(F_o^2 - F_c^2)^2$, where $w = [\sigma(F_o^2)]^2 + (0.0166)^2 + 0.82\text{P}^{-1}$ and $P = (F_o^2 + 2F_c^2)/3$. Sm1 and Sm2 were disordered; these atoms were partitioned over two positions. The site occupancy factors (SOFs) of these positions were refined subject to the constraints that the sum of the SOFs for each pair was equal to one, and the anisotropic displacement parameters

of the disordered pairs were restrained to have the same U_{ij} components within an effective

standard deviation of 0.002 Å^2; the SOFs for the major sites refined to 0.91069 for Sm1a and

0.08931 for Sm2a. Hydrogen atoms attached to boron were located in the difference maps, and

their positions were refined with independent isotropic displacement parameters. B-H bond

distances were restrained to be equal within 0.001 Å. Analysis of the diffraction intensities

suggested slight inversion twinning; therefore, the intensities were calculated from the equation I

$= xI_a + (1-x)I_b$, where x is a scale factor that relates the volumes of the inversion-related twin

components. The scale factor refined to a value of 0.29(1). Successful convergence was indicated

by the maximum shift/error of 0.000 for the last cycle. Final refinement parameters are given in

Table 1. The largest peak and deepest hole in the final Fourier difference map were 0.51 eÅ^{-3} and

-0.92 eÅ^{-3} respectively; the former was located 0.88 Å from B5. A final analysis of variance

between observed and calculated structure factors showed no apparent errors.

Tm(H$_3$BNMe$_2$BH$_3$)$_2$(thf)$_3$ and **Tm(H$_3$BNMe$_2$BH$_3$)$_2$(thf)$_2$, 4** and **5**: The monoclinic lattice

and the systematic absences $h0l$, $l \neq 2n$, and $0k0$, $k \neq 2n$, were uniquely consistent with the space

group $P2_1/c$. The structure was solved by direct methods (SHELXTL). Correct positions for the

thulium atoms were deduced from an E-map; subsequent least-squares refinement and difference

Fourier calculations revealed the positions of the remaining non-hydrogen atoms. The quantity

minimized by the least-squares program was $\Sigma w(F_o^2 - F_c^2)^2$, where $w = [\sigma(F_o^2)]^2 + (0.0000P)^2 +$

$40.00P^{-1}$ and $P = (F_o^2 + 2F_c^2)/3$. The thf ligands attached to **5** were disordered over two sites. The

oxygen-carbon bond distances within the disordered thf groups were restrained to be equal within

0.001 Å; a similar restraint was placed on the carbon-carbon bond distances of the disordered thf

groups. The anisotropic displacement parameters of carbon atoms within 1.7 A of other carbon

atoms were restrained to have the same U_{ij} components within an effective standard deviation of

0.01 Å^2. Hydrogen atoms attached to boron were located in the difference maps, and their positions were refined with independent isotropic displacement parameters. No correction for isotropic extinction was necessary. Successful convergence was indicated by the maximum shift/error of 0.000 for the last cycle. Final refinement parameters are given in Table 1. The largest peak in the final Fourier difference map (2.81 eÅ^{-3}) was located 0.79 Å from Tm2. A final analysis of variance between observed and calculated structure factors showed no apparent errors.

Table 2.6. Crystallographic data for the new Sm compounds, **1**, **2**, and **3** at 100 K.

	1	**2**	**3**
formula	$C_{16}H_{48}B_4N_2O_3Sm$	$C_{12}H_{44}B_4N_2O_4Sm$	$C_{16}H_{48}B_2N_2O_6Sm$
FW (g mol^{-1})	510.17	474.09	536.54
λ (Å)	0.71073	0.71073	0.71073
crystal system	orthorhombic	orthorhombic	Monoclinic
space group	*Pbca*	*C*222$_1$	*P*2$_1$
a (Å)	16.6137(5)	10.2515(4)	9.6605(2)
b (Å)	17.3201(6)	14.3867(5)	16.3082(4)
c (Å)	18.0253(6)	28.0995(10)	16.9112(4)
β (deg)	90	90	93.8145(3)
V (Å^3)	5186.8 (4)	4144.2(4)	2658.38
Z	8	4	4
ρ$_{calc}$ (g cm^{-3})	1.307	1.201	1.387
μ (mm^{-1})	2.28	1.46	2.24
R$_{int}$	0.0381	0.0477	0.0314
Absorption correction	multi-scan	multi-scan	multi-scan
Max. min. transm. factors	0.745, 0.554	0.746, 0.596	0.611, 0.423
goodness-of-fit on F^2	1.369	1.090	1.150
R$_1$ [*I*>2σ(*I*)]^a	0.0528	0.0282	0.0157
wR$_2$ (all data)^b	0.1234	0.0666	0.0395

Table 2.7. Crystallographic data for **4** and **5** at 198 K.

	4 and 5
formula	$C_{28}H_{88}B_8N_4O_5Tm_2$
FW (g mol^{-1})	985.38
λ (Å)	0.71073
crystal system	monoclinic
space group	$P2_1/c$
a (Å)	16.7425(5)
b (Å)	11.3406(3)
c (Å)	25.6843(8)
β (deg)	101.9402(6)
V (Å^3)	4771.2(4)
Z	4
ρ_{calc} (g cm^{-3})	1.372
μ (mm^{-1})	3.73
R (int)	0.0507
Absorption correction	multi-scan
Max. min. transm. factors	0.84, 0.38
goodness-of-fit on F^2	1.089
$R1$ [I>2σ(I)]^a	0.0423
$wR2$ (all data)^b	0.0884

References

1.   Asprey, L. B.; Kruse, F. H., Divalent Thulium. Thulium Di-iodide. *J. Inorg. Nucl. Chem.* **1960,** *13*, 32-35. DOI: 10.1016/0022-1902(60)80232-1

2.   Bochkarev, M. N.; Fedushkin, I. L.; Fagin, A. A.; Petrovskaya, T. V.; Ziller, J. W.; Broomhall-Dillard, R. N. R.; Evans, W. J., Synthesis and Structure of the First Molecular Thulium(II) Complex: [TmI$_2$(MeOCH$_2$CH$_2$OMe)$_3$]. *Angew. Chem. Int. Ed. Engl.* **1997,** *36*, 133-135. DOI: 10.1002/anie.199701331

3.   Nief, F.; Turcitu, D.; Ricard, L., Synthesis and Structure of Phospholyl- and Arsolylthulium(II) Complexes. *Chem. Commun.* **2002**. DOI: 10.1039/B204337H

4.   Turcitu, D.; Nief, F.; Ricard, L., Structure and Reactivity of Homoleptic Samarium(II) and Thulium(II) Phospholyl Complexes. *Chem. Eur. J.* **2003,** *9*, 4916-4923. DOI: 10.1002/chem.200305107

5.   Momin, A.; Bonnet, F.; Visseaux, M.; Maron, L.; Taktas, J.; Ferguson, M. J.; Le Goff, X.; Nief, F., Synthesis and Structure of Divalent Thulium Borohydrides and their Application in ε-caprolactone polymerization. *Chem. Commun.* **2011,** *47*, 12203-12205. DOI: 10.1039/c1cc15294g

6.   Evans, W. J.; Allen, N. T.; Ziller, J. W., Expanding Divalent Organolanthanide Chemistry: The First Organothulium(II) Complex and the In Situ Organodysprosium(II) Reduction of Dinitrogen. *Angew. Chem. Int. Ed.* **2002,** *41*, 359-361. DOI: 10.1002/1521-3773(20020118)41:2<359::AID-ANIE359>3.0.CO;2-A

7.   Fedushkin, I. L.; Girgsdies, F.; Schumann, H.; Bochkarev, M. N., Formation and Structure of Thulium(III) Cyclopentadienides as Products of Reactions Directed Towards the Synthesis of Thulium(II) Cyclopentadienides. *Eur. J. Inorg. Chem.* **2001,** *9*. DOI: 10.1002/1099-0682(200109)2001:9<2405::AID-EJIC2405>3.0.CO;2-N

8.   Evans, W. J.; Allen, N. T., Ketone Coupling with Alkyl Iodides, Bromides, and Chlorides Using Thulium Diiodide: A More Powerful Version of $SmI_2(thf)_x$/HMPA. *J. Am. Chem. Soc.* **2000,** *122*, 2118-2119. DOI: 10.1021/ja992951m

9.   Teo, R. D.; Termini, J.; Gray, H. B., Lanthanides: Applications in Cancer Diagnosis and Therapy. *J. Med. Chem.* **2017,** *59*, 6012-6024. DOI: 10.1021/acs.jmedchem.5b01975

10.   Cieszykowska, I.; Zóltowska, M.; Mielcarski, M., Separation of Ytterbium from ^{177}Lu/Yb Mixture by Electrolytic Reduction and Amalgamation. *SOP Transactions on Applied Chemistry* **2014,** *1*, 6-13. DOI: 10.15764/STAC.2014.02002

11.   Preston, J. S.; Preez, A. C., The Separation of Europium from a Middle Rare Earth Concentrate by Combined Chemical Reduction, Precipitation, and Solvent-Extraction Methods. *J. Chem. Tech. Biotechnol.* **1995,** *65*, 93-101. DOI: 10.1002/(SICI)1097-4660(199601)65:1<93::AID-JCTB393>3.0.CO;2-O

12.   Neary, C. R.; Highley, D. E., The Economic Importane of the Rare Earth Elements. In *Developments in Geochemistry*, Henderson, P., Ed. Elsevier: 1984; Vol. 2.

13.   Preinfalk, C.; Morteani, G., The Industrial Applications of Rare Earth Elements. In *Lanthanides, Tantalum and Niobium: Mineralogy, Geochemistry, Characteristics of Primary Ore Deposits, Prospecting, Processing and Applications*, Möller, P.; Černy, P.; Saupé, F., Eds. Springer-Verlag Berlin Heidelberg GmbH: Berlin, 1989.

14.   Gupta, C. K.; Krishnamurthy, N., *Extractive Metallurgy of Rare Earths*. CRC Press: Boca Raton, FL, 2005.

15.   Marsh, J. K., 142. Rare-earth Metal Amalgams. Part IV. The Isolation of Europium. *J. Chem. Soc.* **1943**, 531-535. DOI: 10.1039/JR9430000531

16.   Onstott, E. I., The Separation of Europium from Samarium by Electrolysis. *J. Am. Chem. Soc.* **1955,** *77*, 2129-2132. DOI: 10.1021/ja01613a027

17.   Yntema, L. F., The Separation of Europium by Electrolytic Reduction. Observation on the Rare Earths. XXXV. *J. Am. Chem. Soc.* **1930,** *52*, 2782-2784. DOI: 10.1021/ja01370a030

18.   Ball, R. W.; Yntema, L. F., The Separation of Ytterbium by Electrolytic Reduction. Observations on the Rare Earths. XXXVI. *J. Am. Chem. Soc.* **1930,** *52*, 4264-4268. DOI: 10.1021/ja01374a011

19.   Onstott, E. I., Separation of the Lanthanons at Amalgam Cathodes. IV. High Purity Ytterbium from Mixtures of Heavy Lanthanons by Aqueous Electrolysis. *Anal. Chem.* **1960,** *33*, 1470-1473. DOI: 10.1021/ac60179a006

20.   Bilewicz, A.; Zuchowska, K.; Barbara, B., Separation of Yb as $YbSO_4$ from a ^{176}Yb Target for Prodution of ^{177}Lu via the ^{176}Yb (n, γ) $^{177}Yb \rightarrow ^{177}Lu$ Process. *J. Radioanal. Nucl. Chem.* **2009,** *280*, 167-169. DOI: 10.1007/s10967-008-7437-7

21.   Xin, W.; Deng, Y.; Jiang, Y.; Guo, G., Enhanced Separation of Sm and La from Sm_2O_3-La_2O_3 Mixtures Based on a Reduction-Oxidation Method. *Metall. Mater. Trans. B* **2019,** *50B*, 22-26. DOI: 10.1007/s11663-018-1457-7

22.   Marsh, J. K., 10. Isolation of Samarium, Europium, and Ytterbium Materials by Means of Sodium Amalgam. In *Inorganic Syntheses*, Moeller, T., Ed. McGraw-Hill Book Company: 1957, 1957; Vol. 5.

23.   Fieser, M. E.; Ferrier, M. G.; Su, J.; Batista, E.; Cary, S. K.; Engle, J. W.; Evans, W. J.; Lezama Pacheco, J. S.; Kozimor, S. A.; Olson, A. C.; Ryan, A. J.; Stein, B. W.; Wagner, G.

L.; Woen, D. H.; Vitova, T.; Yang, P., Evaluating the Electronic Structure of Formal Ln^{II} Ions in $Ln^{II}(C_5H_4SiMe_{-3})_3^{-1}$ Using XANES Spectroscopy and DFT Calculations. *Chem. Sci.* **2017,** *8*, 6076-6091. DOI: 10.1039/c7sc00825b

24.   Fieser, M. E.; MacDonald, M. R.; Krull, B. T.; Bates, J. E.; Ziller, J. W.; Furche, F.; Evans, W. J., Structural, Spectroscopic, and Theoretical Comparison of Traditional vs Recently Discovered Ln^{2+} Ions in the $[K(2.2.2\text{-cryptand})][(C_5H_4SiMe_3)_3Ln]$ Complexes: The Variable Nature of Dy^{2+} and Nd^{2+}. *J. Am. Chem. Soc.* **2014,** *137*, 369-382. DOI: 10.1021/ja510831n

25.   MacDonald, M. R.; Bates, J. E.; Ziller, J. W.; Furche, F.; Evans, W. J., Completing the Series of +2 Ions for the Lanthanide Elements: Synthesis of Molecular Complexes of Pr^{2+}, Gd^{2+}, Tb^{2+}, and Lu^{2+}. *J. Am. Chem. Soc.* **2013,** *135*, 9857-9868. DOI: 10.1021/ja403753j

26.   Jaroschik, F.;   Nief, F.;   Le Goff, X.-F.;   Ricard, L., Isolation of Stable Organodysprosium(II) Complexes by Chemical Reduction of Dysprosium(III) Precursors. *Organometallics* **2007,** *26*, 1123-1125. DOI: 10.1021/om0700213

27.   Daly, S. R.; Girolami, G. S., Synthesis, Characterization, and Structures of Divalent Europium and Ytterbium *N,N*-Dimethylaminodiboranates. *Inorg. Chem.* **2010,** *49*, 4578-4585. DOI: 10.1021/ic100292u

28.   Girard, P.;   Namy, J. L.; Kagan, H. B., Divalent Lanthanide Derivatives in Organic Synthesis. 1. Mild Preparation of Samarium Iodide and Ytterbium Iodide and their Use as Reducing or Coupling Agents. *J. Am. Chem. Soc.* **1980,** *102*, 2693-2698. DOI: 10.1021/ja00528a029

29.   Evans, W. J.; Gummersheimer, T. S.; Ziller, J. W., Coordination Chemistry of Samarium Diiodide with Ethers Including the Crystal Structure of Tetrahydrofuran-Solvated Samarium Diiodide, $SmI_2(thf)_5$. *J. Am. Chem. Soc.* **1995,** *117*, 8999-9002. DOI: 10.1021/ja00140a016

30.   Evans, W. J.; Allen, N. T.; Ziller, J. W., Facile Dinitrogen Reduction via Organometallic Tm(II) Chemistry. *J. Am. Chem. Soc.* **2001,** *123*, 7927-7928. DOI: 10.1021/ja011282l

31.   Evans, W. J.; Zucchi, G.; Ziller, J. W., Dintrogen Reduction by Tm(II), Dy(II), and Nd(II) with Simple Amide Aryloxide Ligands. *J. Am. Chem. Soc.* **2003,** *125*, 10-11. DOI: 10.1021/ja0211712

32.   Daly, S. R.; Kim, D. Y.; Girolami, G. S., Lanthanide *N,N*-Dimethylaminodiboranates as a New Class of Highly Volatile Chemical Vapor Deposition Precursors. *Inorg. Chem.* **2012,** *51*, 7050-7065. DOI: 10.1021/ic.201852j

33.   Milam, S. N. Actinide Porphyrin Complexes. Ph. D. Thesis, University of Illinios Urbana Champaign, 1989.

34.   Samata, H.; Wada, N.; Ozawa, T. C., Van Vleck Paramagnetism of Europium Hydroxide. *Journal of Rare Earths* **2015,** *33*, 177-181. DOI: 10.1016/S1002-0721(14)60399-9

35.   Bren, K. L., Nuclear Magnetic Resonance (NMR) Spectroscopy of Metallobiomolecules. In *Encyclopedia of Inorganic Chemistry*, John Wiley & Sons, Ltd: 2008; pp 1-28.

36.   Dunbar, A. C. High Coordination Number Compounds of Thorium Borohydride and of Calcium and Strontium *N,N*-Dimethylaminodiboranates. Ph.D. Thesis, University of Illinois Urbana-Champaign, 2014.

37.   Daly, S. R.; Bellott, B. J.; Nesbit, M. A.; Girolami, G. S., Synthesis and Structural Diversity of Barium (*N,N*-Dimethylamino)diboranates. *Inorg. Chem.* **2012,** *51*, 6449-6459. DOI: 10.1021/ic2016879

38.   Daly, S. R.; Kim, D. Y.; Yang, Y.; Abelson, J. R.; Girolami, G. S., Lanthanide *N,N*-Dimethylaminodiboranates: Highly Volatile Precursors for the Deposition of Lanthanide-Containing Thin Films. *J. Am. Chem. Soc.* **2010,** *132*, 2106-2107. DOI: 10.1021/ja9098005

39.   Daly, S. R.; Girolami, G. S., Synthesis, Characterization, and Structure of Uranium(III) *N,N*-Dimethylaminodiboranates. *Inorg. Chem.* **2010,** *49*, 4578-4585. DOI: 10.1021/ic100292u

40.   Daly, S. R.; Piccoli, P. M.; Schultz, A. J.; Todorova, T. K.; Gagliardi, L.; Girolami, G. S., Synthesis and Properties of a Fifteen Coordinate Complex: the Thorium Aminodiboranate Th(H$_3$BNMe$_2$BH$_3$)$_4$. *Angew. Chem.* **2010,** *49*, 3379-3381. DOI: 10.1002/anie.200905797

41.   Kim, D. Y. Part I. Synthesis of Metal Hydroborates as Potential Chemical Vapor Deposition Precursors Part II. Chemical Vapor Deposition of Titanium-Doped Magnesium Diboride Thin Films. Ph. D. Thesis, University of Illinois Urbana Champaign, 2007.

42.   Marks, T. J.; Kennelly, W. J.; Kolb, J. R.; Shimp, L. A., Structure and Dynamics in Metal Tetrahydroborates. II. Vibrational Spectra and Structures of Some Transition Metal and Actinide Tetrahydroborates. *Inorg. Chem.* **1972,** *11*, 2540-2546. DOI: 10.1021/ic50116a051

43.   Clark, R. J. H.; Machin, D. J.; Lewis, J.; Nyholm, R. S., Complexes of Titanium Trichloride. *J. Chem. Soc.* **1963**, 379-387. DOI: 10.1039/jr9630000379

44.   Heljer, M. D.; Driessen, W. L., Ethers as Ligands. Part II. Metal(II) Dimethoxyethane Solvates. *Inorganica Chim. Acta* **1978,** *26*, 227-230. DOI: 10.1016/S0020-1693(00)87219-9

45.   Snyder, R. G.; Zerbi, G., Vibrational Analysis of Ten Simple Aliphatic Ethers: Spectra, Assignments, Valence Force Field and Molecular Conformations. *Spectrochim. Acta A* **1967**, 391-437. DOI: 10.1016/0584-8539(67)80241-1

46.   Jaroschik, F.; Bonnet, F.; Le Goff, X.; Ricard, L.; Nief, F.; Visseaux, M., Synthesis of Samarium(II) Borohydrides and their Behavior as Initiators in Styrene and ε-Caprolactone Polymerization. *Dalton Trans.* **2010,** *39*, 6761-6766. DOI: 10.1039/c001795g

47.   Evans, W. J.; Drummond, D. K.; Zhang, H.; Atwood, J. L., Synthesis and Structure of the Divalent   [Bis(trimethylsilyl)amido]samarium   Complexes $[(Me_3Si)_2N]_2Sm(thf)_2$ and $\{[Me_3Si)_2N]Sm(\mu\text{-}I)(dme)(thf)\}_2$. *Inorg. Chem.* **1988,** *27*, 575-579. DOI: 10.1021/ic00276a027

48.   Evans, W. J.; Grate, J. W.; Choi, H. W.; Bloom, I.; Hunter, W. E.; Atwood, J. L., Solution Synthesis and Crystollographic Characterization of the Divalent Organosamarium Complexes $(C_5Me_5)_2Sm(thf)_2$ and $[(C_5Me_5)Sm(\mu\text{-}I)(thf)_2]_2$. *J. Am. Chem. Soc.* **1985,** *107*, 941-946. DOI: 10.1021/ja00290a032

49.   Hitzbleck, J.; Deacon, G. B.; Ruhlandt-Senge, K., Linear Finite "Mers"-Homoleptic Polynuclear Heavy Alkaline Earth Metal Pyrazolates. *Angew. Chem. Int. Ed.* **2004,** *43*, 5218-5220. DOI: 10.1002/anie.200460628

50.   Cheng, J.; Taktas, F.; Ferguson, M. J.; McDonald, R., Heteroleptic Tm(II) Complexes: One More Success for Trofimenko's Scorpionates. *J. Am. Chem. Soc.* **2008,** *130*, 1544-1545. DOI: 10.1021/ja0776273

51.   Shannon, R. D., Revised Effective Ionic Radii and Systematic Studies of Interatomic Distances in Halides and Chalcogenides. *Acta Cryst. A* **1976,** *A32*, 751-767. DOI: 10.1107/S0567739476001551

52.   Rogers, R. D.; Kurihara, L. K., f-Element/Crown Ether Complexes. 4. Synthesis and Crystal and Molecular Structures of $[MCl(OH_2)_2(18\text{-crown-}6)]Cl_2 \cdot 2\ H_2O$ (M=Sm, Gd, Tb). *Inorg. Chem.* **1987,** *26*, 1498-1502. DOI: 10.1021/ic00257a008

53.   Starynowlcz, P., Two Complexes of Sm(II) with Crown Ethers-Electrochemical Synthesis, Structure and Spectroscopy. *Dalton Trans.* **2004**, 825-832. DOI: 10.1039/b316253b

54.   Gun'ko, Y. K.; Hitchcock, P. B.; Lappert, M. F., Displacement of a Cyclopentadienyl Ligand by a Crown Ether from a Lanthanocene (II) [LnCp"$_2$]; Crystal Structures of the First Cationic Lanthanoid(II) Complexes [SmCp"([18]-crown-6)][SmCp"$_3$]•0.5 C$_6$H$_6$ and [YbCp"([18]-crown-6)][Cp"]•3 C$_6$H$_6$ [Cp" = η^5-C$_5$H$_3$(SiMe$_3$)$_2$-1,3]. *Chem. Commun.* **1998**, 1843-1844. DOI: 10.1039/A805544K

55.   Bestgen, S.; Chen, Q.; Rees, N. H.; Goicoechea, J. M., Synthesis and Reactivity of Rare-Earth Metal Phosphaethynolates. *Dalton Trans.* **2018,** *47*, 13016-13024. DOI: 10.1039/c8dt03427c

56.   Edelstein, N., Bonding in Metal Borohydride Complexes. *Inorg. Chem.* **1981,** *20*, 297-299. DOI: 10.1021/ic50215a068

57.   Hitzbleck, J.; O'Brien, A. Y.; Deacon, G. B.; Ruhlandt-Senge, K., Role of Donor and Secondary Interactions in the Structures and Thermal Properties of Alkaline-Earth and Rare-Earth Metal Pyrazolates. *Inorg. Chem.* **2006,** *45*, 10329-10337. DOI: 10.1021/ic061294d

58.   Studebaker, D. B.; Neumayer, D. A.; Hinds, B. J.; Stern, C. L.; Marks, T. J., Encapsulating Bis(β-Ketoiminato) Polyethers. Volatile, Fluorine-Free Barium Precursors for Metal-Organic Chemical Vapor Deposition. *Inorg. Chem.* **2000,** *39*, 3148-3157. DOI: 10.1021/ic991161a

59.   El-Kaderi, H. M.; Heeg, M. J.; Winters, C. H., Synthesis, Structure, and Properties of Monomeric Strontium and Barium Complexes Containing Terminal η^2-3,5-Di-tert-butylpyrazolato Ligands. *Polyhedron* **2005,** *24*, 645-653. DOI: 10.1016/j.poly.2005.01.011

60.   Noth, H.; Thomas, S., Metal Tetrahydridoborates and Tetrahydroborato Metallates, 24 Solvates of Sodium Bis(borane)dimethylamide. *Eur. J. Inorg. Chem.* **1999**, 1373-1379. DOI: 10.1002/(SICI)1099-0682(199908)1999:8<1373::AID-EJIC1373>3.0.CO;2-7